UNIVERSITY OF HELSINKI REPORT SERIES IN PHYSICS

HU-P-D151

Simulations of dimensionally reduced effective theories of high temperature QCD

ARI HIETANEN

Division of Elementary Particle Physics
Department of Physics
Faculty of Science
University of Helsinki
Helsinki, Finland

ACADEMIC DISSERTATION
To be presented, with the permission of the Faculty of Science of the University of Helsinki, for public criticism in Auditorium CK112 at Exactum, Gustaf Hällströmin katu 2b, on Friday, April 25th, 2008, at 12 o'clock.

Helsinki 2008

ISBN 978-952-10-3928-7 (printed version)
ISSN 0356-0961
ISBN 978-952-10-3929-4 (pdf-version)
http://ethesis.helsinki.fi
Yliopistopaino
Helsinki 2008

Preface

This thesis is based on research carried out at the *Theoretical Physics Division* of the *Department of Physics* in the University of Helsinki, URHIC theory project at the Helsinki Institute of Physics and CERN during the past five years. It has been funded by the Academy of Finland, Contract no. 77744, 104382 and 114371, as well as the Magnus Ehrnrooth foundation and the Marie Curie Host Fellowship for Early Stage Researches Training. In addition I have been a member of the *Finnish Graduate School of Particle and Nuclear Physics* (GRASPANP) as well as the *Field Theory at Finite Temperature and Density* group of the University of Helsinki.

First of all I want to thank my supervisor Prof. Kari Rummukainen for his invaluable instructions and suggestions. I am also grateful to Prof. Keijo Kajantie for his guidance. I also want to thank my colleague and friend Aleksi Kurkela. The collaboration with him has been the most enjoyable part of the work. The referees of my thesis, Kari J. Eskola and Aleksi Vuorinen have also given me constructive and useful comments on this manuscript for which I'm grateful. In addition, I want to thank Mikko Laine and York Schröder.

My friends and colleagues, Antti Gynther, Janne Högdahl, Tuomas Lappi, Vesa Muhonen, Sami Nurmi, Mikael Ottela, Olli Taanila, Mikko Vepsälainen, Antti Väihkonen and many other have made my time at the department most enjoyable.

Last, I want to express my gratitude to my parents and to my brother Eero and sister Sanni for constant support during my work, and to Ying-Chan for her love and care.

Helsinki, March 2008

Ari Hietanen

A. Hietanen: Simulations of dimensionally reduced effective theories of high temperature QCD, University of Helsinki, 2008, 54 p. + appendices, Report Series in Physics, HU-P-D151 , ISSN 0356-0961, ISBN 978-952-10-3928-7 (printed version), ISBN 978-952-10-3929-4(pdf version).
INSPEC classification: A1110N, A1110W,
Keywords: quantum chromodynamics, quark-gluon plasma, finite-temperature field theory, effective field theory, lattice QCD.

Abstract

Quantum chromodynamics (QCD) is the theory describing interaction between quarks and gluons. At low temperatures, quarks are confined forming hadrons, e.g. protons and neutrons. However, at extremely high temperatures the hadrons break apart and the matter transforms into plasma of individual quarks and gluons.

In this theses the quark gluon plasma (QGP) phase of QCD is studied using lattice techniques in the framework of dimensionally reduced effective theories EQCD and MQCD. Two quantities are in particular interest: the pressure (or grand potential) and the quark number susceptibility. At high temperatures the pressure admits a generalised coupling constant expansion, where some coefficients are non-perturbative. We determine the first such contribution of order g^6 by performing lattice simulations in MQCD. This requires high precision lattice calculations, which we perform with different number of colors N_c to obtain N_c-dependence on the coefficient.

The quark number susceptibility is studied by performing lattice simulations in EQCD. We measure both flavor singlet (diagonal) and non-singlet (off-diagonal) quark number susceptibilities. The finite chemical potential results are optained using analytic continuation. The diagonal susceptibility approaches the perturbative result above $20T_\mathrm{c}$, but below that temperature we observe significant deviations. The results agree well with 4d lattice data down to temperatures $2T_\mathrm{c}$.

Contents

Preface . . . i
Abstract . . . ii
List of included papers . . . v

1 Introduction **1**

2 Finite temperature QCD **4**
2.1 Basics of quantum field thermodynamics . . . 4
2.2 Finite temperature quantum chromodynamics . . . 5

3 Pressure of QCD up to order g^6 **8**
3.1 Limitations of perturbation theory . . . 8
3.2 Dimensional reduction . . . 11
3.3 Validity of dimensional reduction . . . 16

4 Calculations of $B_{\rm G}(N_{\rm c})$ **19**
4.1 EQCD on the lattice . . . 19
4.2 Lattice $\overline{\rm MS}$ relation for $B_G(N_c)$ . . . 21
4.2.1 Large-$N_{\rm c}$ limit . . . 22
4.3 Lattice simulations . . . 23
4.3.1 Simulation algorithms . . . 23
4.3.2 The simulations . . . 25
4.3.3 Accuracy requirements . . . 26
4.3.4 The result . . . 27
4.4 Consistency of the result . . . 29

5 The diagonal and off-diagonal quark number susceptibilities **30**
5.1 Susceptibilities in EQCD . . . 30
5.2 The finite density simulations . . . 31
5.2.1 Reweighting . . . 31
5.2.2 Taylor expansion . . . 32
5.2.3 Analytic continuation . . . 32
5.2.4 Imaginary μ and the phase diagram of EQCD . . . 33
5.3 Matching to QCD . . . 33
5.4 Lattice $\overline{\rm MS}$ relations for condensates K_i . . . 34
5.5 Simulation algorithms . . . 35
5.6 Results of lattice simulations . . . 36
5.6.1 Diagonal susceptibility . . . 36

5.6.2 Off-diagonal susceptibility 37

6 Conclusions and Outlook **41**

A Lattice perturbation theory **43**
A.1 Plaquette expectation value 43
A.2 Lattice integrals in EQCD 46

List of included papers

The three articles included in this thesis are [1, 2, 3]:

[1] A. Hietanen, K. Kajantie, M. Laine, K. Rummukainen, Y. Schroder, *Plaquette expectation value and gluon condensate in three dimensions*, JHEP **01** (2005) 013, [hep-lat/0412008].

[2] A. Hietanen, A. Kurkela, *Plaquette expectation value and lattice free energy of three-dimensional SU(N) gauge theory*, JHEP **11** (2006) 060, hep-lat/0609015.

[3] A. Hietanen, K. Rummukainen, *The diagonal and off-diagonal quark number susceptibility of high temperature and finite density QCD*, accepted to be published in JHEP, [arXiv:0802.3979].

My contribution to the publications: In Ref. [1] I performed part of the simulations, did the numerical analysis and checked some calculations of lattice perturbation theory. In Ref. [2], I wrote some simulation codes used, ran part of the simulations and performed the numerical analysis. In Ref. [3], I wrote certain parts of simulation code, and performed the numerical simulations and the analysis. I also derived matching equations between EQCD and QCD and some of the lattice-$\overline{\text{MS}}$ matching equations applied. In the second and the third paper I also wrote the first draft. The polishing of the papers were done jointly.

There are also three conference proceedings Ref. [4, 5, 6], which are closely related to this work, but not included in the thesis.

Chapter 1

Introduction

At the era of new particle accelerators like Tevatronin Fermilab, Relativistic Heavy Ion Collider (RHIC) in Brookhaven and the upcoming Large Hadron collider (LHC) in CERN, experimental particle physics is at the verge of new findings, which might include the Higgs boson and supersymmetry among others. It is also hoped that one would gather some evidence for or against more controversial predictions, such as string theory and extra dimensions. In addition to new findings, the experiments are expected to provide a more profound understanding of an already accepted theory, the theory of strong interactions, quantum chromodynamics (QCD).

QCD was developed in the mid seventies, but the first discoveries leading to it date back to 1964 when Gell-Mann [7] and Zweig [8] proposed a model that explains the hadron spectroscopy in terms of elementary constituents, quarks. Mesons were expected to be quark-antiquark bound states and baryons bound states of three different quarks. By assuming three different species of quarks, which have fractional charges and spin 1/2, Gell-Mann and Zweig were able to explain the quantum numbers of all the hadrons known by then. Later, the number of different quark types, which are usually referred to as flavors, has grown to six.

There were two problems in the quark model. First, the spectrum of baryons included particles, which should not exist according to Fermi-Dirac statistic, for example Δ^{++} which consisted of three up-quarks. This problem was solved by Han and Nambu [9], Greenberg [10], and Gell-Mann by proposing that quarks carry an additional, unobserved quantum number called color. The simplest model of color would be to assign quarks to the fundamental representation of a new, internal global SU(3) symmetry.

The second problem was that the individual quarks were never seen. Hence, all the observed particles were color singlets. This problem was solved when Gross and Wilczek, and independently Politzer discovered [11, 12] that non-Abelian gauge theories were asymptotically free, meaning that the coupling constant approaches zero as the the energy increases. Conversely, as the quarks are stretched apart the coupling constant grows. This may then lead to interactions which are sufficiently strong to prevent individual quarks from escaping. Then, the color symmetry, having no other physical meaning, was identified as the symmetry associated with asymptotic freedom. The colors were quantum numbers of quarks. This resulted in a theory of strong interactions called QCD as a system of quarks, which had various flavors and were each assigned to the fundamental representation of the local gauge group $SU(3)$. The quanta of the $SU(3)$ gauge fields are called gluons, and the property which ensures that individual quarks or gluons are never seen, is called confinement. There is no rigorous mathematical proof that QCD is a confining theory. Nevertheless, it has been shown to be true by lattice techniques [13].

However, as predicted by lattice calulations [14, 15, 16], at extremely high temperatures or

densities the hadrons break apart and the matter transforms into a plasma of individual quarks and gluons. The plasma is called quark-gluon plasma (QGP). The phase transition occurs at zero chemical potential $\mu = 0$ at temperatures around $T_c \approx 170\text{MeV} \approx 2.0 \times 10^{12}\text{K}$. One of the most essential goals of experimental and theoretical particle physics currently is to understand the properties of QGP. At much higher temperatures than T_c, one expects QGP to behave as an ideal gas because the coupling approaches zero as temperature increases. However, this argument does not hold down to temperatures near the phase transition, where the coupling constant grows larger. For example, the recent observations at RHIC [17] suggest that the QGP behaves as a perfect liquid, which implies strong coupling. Also, lattice simulations have found expectation values for, e.g., pressure [18], far from ideal gas, and even in perturbation theory one observes a significant deviation from ideal gas results at temperatures as high as $1000T_c$.

One major problem in the theoretical understanding of QGP is the large difference between the results from perturbative calculations and lattice simulations. The lattice results grow more expensive as temperatures increase[1] because the simulation parameters must fulfill a wide range of conditions. First, the lattice spacing a must be much smaller than the periodic time direction $1/T$, which in this case is much smaller than T_c, and T_c must be much smaller than the lattice size L. In addition, in the calculation of the equation of state or grand potential $\Omega = -pV$, there is the problem of infinite zero energy, which is normalized by subtracting the corresponding zero temperature result, which has to be calculated on a lattice larger than the inverse of the typical QCD energy scale, $1/\Lambda_{\overline{\text{MS}}}$.

Naturally, perturbation theory does not work at low temperatures, because the running coupling constant is not small around T_c and decreases only logarithmically as T increases. One could hope that the calculation of additional terms in perturbation theory would bring the results closer to lattice results. But in addition to the calculations becoming prohibitively more difficult at each new loop order, there is a fundamental barrier, which arises at some order in g and depends on the observable in case. For example, in the case of the pressure p, the order is g^6 and for the quark number susceptibility g^8. The barrier is due to infrared problems, which cause all the orders of loop expansion to contribute at the same order of expansion in the coupling constant. It was first discovered by Linde [19].

The size of the non-perturbative effects could be estimated by lattice calculations, but this would require simulations at extremely high temperatures for the results to be comparable with perturbation theory. Therefore, it is not a feasible option. However, we can utilize the effective field theory methods and construct a simpler theory, which exhibits the same infrared behaviour as the full theory. The derivation of the effective theory is based on the fact that at sufficiently high temperatures QCD has three relevant energy scales: πT, gT and g^2T. Thus, we can perturbatively integrate over scale πT, obtaining a theory for scales gT and g^2T only. Because all of the field modes which exhibit (imaginary) time dependence and all fermion field modes have effective masses of $\pi T \gg gT$, g^2T, the effective theory is three dimensional and purely bosonic, called electrostatic QCD (EQCD). This procedure is often called dimensional reduction. All the parameters of EQCD are perturbatively matched to the parameters of full QCD making it an effective theory. One can also continue the procedure and integrate out the modes proportional to gT, which results in an effective theory called magnetostatic QCD (MQCD). MQCD is a 3d pure gauge theory and includes all infrared sensitive contributions which are not calculable in perturbation theory.

The dimensionally reduced theories provide an interesting alternative to standard 4d lattice simulations. Above all, they are three dimensional and purely bosonic, making them much

[1]Naturally at T_c the simulations are demanding due to critical slowdown.

cheaper to simulate. They are also superrenormalizable theories so one can calculate the lattice continuum relations exactly. The downside is that the matching back to the full QCD is perturbative and therefore we cannot study, e.g., the phase transition. The methods also allow us to obtain otherwise incalculable corrections to perturbation theory. For example, in the case of pressure, we can perform simulations in MQCD and find the infrared divergent part of the g^6 contribution.

The purpose of this thesis is to study the dimensionally reduced effective theories EQCD and MQCD using lattice methods. The thesis is based on three papers [1, 2, 3]. We are in particular interested in two quantities: the pressure (or grand potential) and the quark number susceptibility. The pressure is one of the most important and fundamental quantities describing the properties of the QGP. Its value is of great importance to the study of heavy-ion collisions. Namely, it describes the expansion and cooling of heavy-ion collision products in terms of hydrodynamics. Hence, it is also relevant to the expansion of the early universe where similar conditions occurred. The quark number susceptibility is related to event-by-event fluctuations in heavy ion collisions and can work as a signature of the formation of the quark gluon plasma [20, 21].

The thesis is organised as follows. In chapter 2, we will introduce the basic concepts of thermal quantum field theory and QCD. In chapter 3, we consider the perturbative calculation of the QCD pressure and also discuss the dimensional reduction. In chapter 4, we review the calculation of the non-perturbative input to the QCD pressure, which we perform in general $N_{\rm c}$. Chapter 5 is devoted to the calculation of susceptibility. Chapter 6 contains our conclusions. Some results of lattice perturbation theory are given in Appendix A.

Chapter 2

Finite temperature QCD

In this chapter we will give a brief introduction to the thermodynamics of quantum fields (see, e.g., [22]). The QCD Lagrangian is discussed at the end of the chapter (see, e.g., [23]).

2.1 Basics of quantum field thermodynamics

To study a statistical system one needs an ensemble which describes the correct macroscopic behaviour. The choice of the ensemble depends on the dynamics and the boundary conditions of the system. For quantum field theory the grand canonical ensemble is a natural choice, because it can change energy as well as particles with an external reservoir allowing particle creation and annihilation. The density matrix for the grand canonical ensemble is

$$\rho(\beta) = e^{-\beta(H-\mu_i N_i)}, \tag{2.1}$$

where β is the inverse of the equilibrium temperature, H is the Hamiltonian and N_i are a set of conserved number operators (assumed to commute with H) and μ_i are chemical potentials. A summation over repeated indices is implied.

Given the density matrix, the ensemble averages are defined through the formula

$$\langle A \rangle = \frac{1}{Z} \mathrm{Tr} \rho A, \tag{2.2}$$

where

$$Z = \mathrm{Tr}\rho \tag{2.3}$$

is the partition function. All standard thermodynamical properties can be derived from this. E.g., the first partial derivatives of Z give

$$P = \frac{T\partial \ln Z}{\partial V}, \qquad N_i = \frac{T\partial \ln Z}{\partial \mu_i} \tag{2.4}$$

$$S = \frac{\partial T \ln Z}{\partial T}, \qquad E = -PV + TS + \mu_i N_i, \tag{2.5}$$

and its second derivatives give, e.g., the susceptibilities, which are particular examples of response functions

$$\chi_{ij} = \frac{\partial^2 \ln Z}{\partial \mu_i \partial \mu_j}. \tag{2.6}$$

Hence, the knowledge of the system can be returned to the knowledge of its partition function. The standard method to calculate partition functions in quantum field theory is the usage of functional integrals or path integrals.

Let $\hat{\phi}(\mathbf{x}, t)$ be the Schrödinger-picture field operator for a neutral scalar field and $\hat{\pi}(\mathbf{x}, t)$ its conjugate momentum. Then Z can be written as

$$Z = \int \mathrm{d}\phi \langle \phi | e^{-\beta(H - \mu_i N_i)} | \phi \rangle, \tag{2.7}$$

where $|\phi\rangle$ is the eigenstate of $\hat{\phi}(\mathbf{x}, 0)$, with eigenvalue $\phi(\mathbf{x})$. This can be interpreted as a transition amplitude from state $|\phi\rangle$ to itself with an imaginary time $\tau = it = 1/T$. Thus, the partition function can be written, in analogy to real time case, as

$$Z = \int \mathcal{D}\pi \int \mathcal{D}\phi \exp\left\{ \int_0^\beta \mathrm{d}\tau \int \mathrm{d}^3 x \left(i\pi(\mathbf{x}, \tau) \frac{\partial \phi(\mathbf{x}, \tau)}{\partial \tau} - \mathcal{H}(\pi, \phi) + \mu_i \mathcal{N}_i(\pi, \phi) \right) \right\}, \tag{2.8}$$

where the field ϕ is constrained so that $\phi(\mathbf{x}, 0) = \phi(\mathbf{x}, \beta)$. In physically interesting cases, the Hamiltonian is usually quadratic in π and the momentum interaction can be carried out, resulting in

$$Z = \int \mathcal{D}\phi \exp\left(\int_0^\beta \mathrm{d}\tau \int \mathrm{d}^3 x \mathcal{L}'(\phi, \dot{\phi}) \right), \tag{2.9}$$

where $\mathcal{L}'$ is the Lagrangian. The same procedure also applies for charged Dirac fields. The major difference is that the fields are now constrained as $\psi(\mathbf{x}, 0) = -\psi(\mathbf{x}, \beta)$, which follows from the anti-commuting property of fermions.

Usually, it is more convenient to work in momentum than in coordinate space. Because of the (anti)periodic boundary conditions in the imaginary time direction, the momentum integration over the imaginary time turns, in fact, into a Fourier series

$$\phi(\mathbf{p}, \tau) = \sqrt{\frac{\beta}{V}} \sum_{n=-\infty}^{\infty} \int \mathrm{d}^3 p e^{i(\omega_n \tau + \mathbf{p}\cdot\mathbf{x})} \phi_n(\mathbf{x}), \tag{2.10}$$

where

$$\omega_n = \begin{cases} 2\pi n T & \text{bosons} \\ 2\pi(n+1)T & \text{fermions} \end{cases} \tag{2.11}$$

The different values of ω_n for bosons and fermions follows from the periodic and anti-periodic boundary conditions.

2.2 Finite temperature quantum chromodynamics

QCD is a renormalizable non-Abelian gauge field theory for the strong interactions. Using standard Euclidean metric $g^{\mu\nu} = \delta^{\mu\nu}$, it is defined through the lagrangian

$$\mathcal{L}_{\mathrm{QCD}} = \frac{1}{4} F^a_{\mu\nu} F^{\mu\nu}_a + \bar{\psi}(\not{D} + M)\psi, \tag{2.12}$$

where the field strength tensor is

$$F^a_{\mu\nu} = \partial_\mu A^a_\nu - \partial_\nu A^a_\mu + g f^{\mathrm{abc}} A^b_\mu A^c_\nu. \tag{2.13}$$

The field strength tensor describes the interaction and propagation of gluons and is invariant under the gauge transformation

$$A_a^\mu T_a \to \Lambda(x)\left(A_a^\mu T_a + \frac{i}{g}\partial^\mu\right)\Lambda^\dagger(x), \tag{2.14}$$

where $\Lambda \in \mathrm{SU}(N_\mathrm{c})$ is

$$\Lambda(x) = \exp(ig\alpha_a(x)T_a). \tag{2.15}$$

The infinitesimal form of a gauge transformation can be derived by expanding in $\alpha(x)$. The result is

$$A_a^\mu \to A_a^\mu + \frac{1}{g}\partial^\mu\alpha_a + gf_{abc}A_b^\mu\alpha_c. \tag{2.16}$$

The antisymmetric structure constants are defined as

$$[T^a, T^b] = if^{abc}T^c, \tag{2.17}$$

where T^a are the generators of $SU(N_\mathrm{c})$ and $a = 1, \ldots, N_\mathrm{c}^2 - 1$. In the physical case of QCD $N_\mathrm{c} = 3$. The generators are normalized as

$$\mathrm{Tr}(T^aT^b) = \frac{1}{2}\delta^{ab} \tag{2.18}$$

The second term in the QCD lagrangian is the fermion lagrangian. It consists of the covariant derivative term

$$\not{D}\psi \equiv i\gamma_\mu\left(\partial_\mu - igA_\mu^a T^a\right)\psi, \tag{2.19}$$

which contains the minimal coupling of the quarks to the gluons. The third term includes the quark mass matrix

$$\mathrm{diag(M)} = (\mathrm{m_u}, \mathrm{m_d}, \mathrm{m_s}, \mathrm{m_c}, \mathrm{m_b}, \mathrm{m_t}). \tag{2.20}$$

We study QCD in the high temperature regime, where at least the lightest quark masses are much lower than the energy scales. On the other hand, if the mass of a quark is $m_f > T$, its contribution to thermodynamical quantities is negligible. Hence we assume from now on the quark masses to be zero and work with a general N_f, which in practise is taken ≤ 3.

The quark field transforms under the finite gauge transformation as

$$\psi(x) \to \Lambda(x)\psi(x), \tag{2.21}$$

and under the infinitesimal gauge transformation as

$$\psi(x) \to (1 + ig\alpha^a(x)T^a)\psi(x). \tag{2.22}$$

We have suppressed the color ($A = 1, .., N_\mathrm{c}$), flavor ($f = 1, .., N_f$), and spinor ($\alpha = 1, .., 4$) index of ψ. With all indices written explicitly, the terms of Lagrangian (2.12) are, e.g, of the form:

$$\bar{\psi}\not{A}\psi = \bar{\psi}^\alpha_{A,f}\gamma^\mu_{\alpha\beta}A^a_\mu T^a_{AB}\psi^\beta_{B,f}. \tag{2.23}$$

We can derive the partition function for QCD at finite temperature and density using the path integral representation. In the path integral the integration is over all gauge configurations, but configurations related to each other under the gauge transformation (2.14) and (2.22) are

physically equivalent. To avoid the overcounting we have to impose a gauge condition. One set of gauges that are often used is the set of covariant gauges

$$F^a = \partial^\mu A^a_\mu - f^a(x) = 0, \tag{2.24}$$

where f^a is a undetermined function. The standard way of imposing the gauge condition is to utilize the Faddeev-Popov procedure [24], which modifies the action so that the gauge condition is in effect. This requires adding additional "ghost " fields η^a and $\bar{\eta}^a$, which are anti-commuting scalars. After some technicalities, we obtain the partition function with gauge fixing terms

$$Z_{\rm QCD} = \int \mathcal{D}A_\mu \mathcal{D}\bar{\psi}\mathcal{D}\psi \exp\left[-\int_0^\beta \mathrm{d}x_0 \int \mathrm{d}^3x \mathcal{L}_{\rm eff}\right], \tag{2.25}$$

where the effective Lagrangian density $\mathcal{L}_{\rm eff}$ is

$$\mathcal{L}_{\rm eff} = \mathcal{L}_{\rm QCD} + \frac{1}{2\xi}(\partial_\mu A^a_\mu)^2 - \sum_f \psi^\dagger_f \mu_f \psi_f + \bar{\eta}^a \left(\partial^2 \delta^{ab} + g f^{abc} A^c_\mu \partial_\mu\right) \eta^b, \tag{2.26}$$

ξ is the gauge parameter. The Faddeev-Popov procedure guarantees that the value of any correlation function of gauge-invariant operators computed from Feynman diagrams will be independent of the value ξ. Thus, it is usually fixed before perturbative calculations. The choice $\xi = 0$ corresponds to the Landau gauge and $\xi = 1$ to the Feynman gauge.

QCD has two remarkable properties. The First is the asymptotic freedom [11, 12], which states that at large enough energies (or short enough distances) the gauge coupling approaches zero. This can be seen from the running of the coupling constant g, which in the lowest order reads

$$g^2(\Lambda) = \frac{24\pi^2}{(11N_{\rm c} - 2N_{\rm f})\ln(\Lambda/\Lambda_{\rm QCD})}, \tag{2.27}$$

where Λ is the renormalization scale and $\Lambda_{\rm QCD} \sim 150$MeV a free parameter corresponding to the characteristic energy scale of the theory.

The second is the confinement, which ensures that individual quarks and gluons are never seen. If one attempts to separate a color-singlet state into colored components, e.g., decompose meson into a quark and an antiquark $q\bar{q}$, the energy cost of separating color sources grows proportionally to the separation. At high enough distance between quarks, the potential energy of the system is greater than required for a creation of a real quark antiquark pair. Hence, by a $q\bar{q}$-pair production the energy of the system is lowered to a new state consisting of color-singlet hadrons. However, at high enough temperatures $T_{\rm c} \sim 170$ MeV or chemical pontentials $\mu \sim 350$ Mev strongly interacting matter appears in a deconfined phase where the quarks are liberated from their confinement [14, 15, 16].

Chapter 3

Pressure of QCD up to order g^6

In this chapter we first review the known results of the QCD perturbative expansion of the pressure and describe the problems and limitations involved in it. The perturbative calculation has been performed up to order $\mathcal{O}\left(g^6 \ln g\right)$, which is the last purely perturbative order. We also explain the ingredients needed to calculate the first non-perturbative order $\mathcal{O}(g^6)$ in the framework of dimensional reduction. We finish this chapter by briefly discussing the region of validity of dimensional reduction.

3.1 Limitations of perturbation theory

The quantity of interest here is minus the free-energy density (grand potential) or the pressure defined by

$$p_{\mathrm{QCD}} \equiv \lim_{V\to\infty} \frac{T}{V} \int \mathcal{D}A_\mu \mathcal{D}\bar{\psi}\mathcal{D}\psi \exp(-S_{\mathrm{QCD}}), \tag{3.1}$$

where S_{QCD} is the QCD action

$$S_{\mathrm{QCD}} = \int \mathrm{d}^4x \mathcal{L}_{\mathrm{QCD}}. \tag{3.2}$$

The running of the coupling constant allows us to perform perturbative calculations at high temperature. In the leading order of perturbation theory ($g = 0$), the QGP is a free gas of gauge bosons and quarks. Hence, the result is the ideal gas result multiplied with the correct number of degrees of freedom. For a finite chemical potential μ, the result called Stefan-Bolzmann law reads:

$$p_{\mathrm{SB}} = \frac{\pi^2 T^4}{45}\left((N_{\mathrm{c}}^2-1)+\frac{7}{4}N_{\mathrm{c}}N_{\mathrm{f}}\right) + \frac{N_{\mathrm{c}}}{6}T^2\sum_f \mu_f^2 + \frac{N_{\mathrm{c}}}{12\pi^2}\sum_f \mu_f^4, \tag{3.3}$$

where $p_{\mathrm{SB}} \equiv p_{\mathrm{QCD}}(g=0)$ and all quark masses have been set to zero.

The complexity of the calculations grows exponentially with each loop order. In Table 3.1 all the calculated orders of the pressure have been listed. The non-analytic terms with odd powers and logarithms of g arise from infrared divergences, which can be cured by calculating all the orders of a specific type of infrared sensitive diagrams. The procedure is called resummation. Braaten and Nieto [25] formulated the problem in such a way that the problematic infrared divergences could be taken into account by the use of dimensionally reduced effective theories.

From the existence of the logarithmic terms, it is obvious that the pressure is not an analytic function of g^2, and therefore there exists no domain of convergence for the expansion parameter $\alpha_{\mathrm{S}} = g^2/(4\pi) > 0$. This was first noted by Dyson already in 1952 for QED [34] with general

Shuryak and Chin 1978 [26, 27]	g^2	2-loop
Kapusta 1979 [28]	g^3	2-loop resummed
Toimela 1983 [29]	$g^4 \ln g$	2-loop resummed
Arnold and Zhai 1994 [30]	g^4	3-loop resummed
Kastening and Zhai 1995 [31]	g^5	3-loop resummed
Kajantie et. al 2002 [32]	$g^6 \ln g$	4-loop using effective 3d-theories
Vuorinen 2003 [33]	$g^6 \ln g$	generalization of [32] to finite μ

Table 3.1: A list of calculated loop orders of QCD pressure p_{QCD}.

physical arguments. Technically, this corresponds to the factorial growth $\sim n!$ of the expansion coefficients (coefficients of different g^n terms). Nonetheless, the series is believed to be asymptotic. This means that there is an optimal number of terms whose inclusion brings the answer close to the actual value of the function in question, and if one then adds additional terms to the series, it deviates from the correct answer more and more. However, the expansion can be made arbitrary close to the correct answer by decreasing the expansion parameter α_{S}. The optimal number of terms depends on the size of the expansion parameter. A crude approximation for the number of terms is $\sim 1/\alpha_{\mathrm{S}}$. It is also important to note that asymptotic expansions are unique. However, the argument is not reversible; many functions may have the same asymptotic expansion.

The motivation to perform perturbation theory in QCD comes from the fact that it works astonishingly well for QED, where the most accurate correspondence between the theoretical predictions and the results from experiments has been achieved [35]. Nevertheless, the situation in QCD is rather different. The size of the QED coupling (at low scales) is 1/137, whereas the the three loop QCD coupling is 0.2 around $2T_{\mathrm{c}}$, meaning that roughly only the five first terms would converge ($1/\alpha_{\mathrm{S}}(2T_{\mathrm{c}}) \approx 5$) to the correct answer[1]. The situation is gradually amended as the temperature increases and around $10T_{\mathrm{c}}$ the $1/\alpha_{\mathrm{S}} \approx 8$, which probably is large enough for perturbation theory to be valid approach. For smaller temperatures, the situation is unclear and the only certain way to find out the soundness of perturbation theory is to actually perform the computation to the next order and compare the result with the previous orders, lattice simulations, and experiments.

However, there is a fundamental barrier in finite temperature perturbation theory that prevents us from calculating the expansion of the pressure up to g^6. The problem was first noted by Linde [19] already at 1980 and it is again due to infrared modes. But this time they are of a more severe type than those cured by the resummations and up until now a purely analytic solution to this problem has not been discovered.

The infrared problems can be understood by considering the order at which the Feynman diagrams contribute. Following Ref. [22], let us examine a $l+1$ loop diagram of the following type:

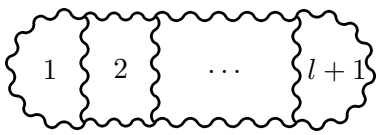

If $l = 1$, there are three propagators and two vertices. Adding a loop adds two vertices and

[1]The value is for $N_{\mathrm{f}} = 2$ with $T_{\mathrm{c}}/\Lambda_{\overline{\mathrm{MS}}} = 0.7$

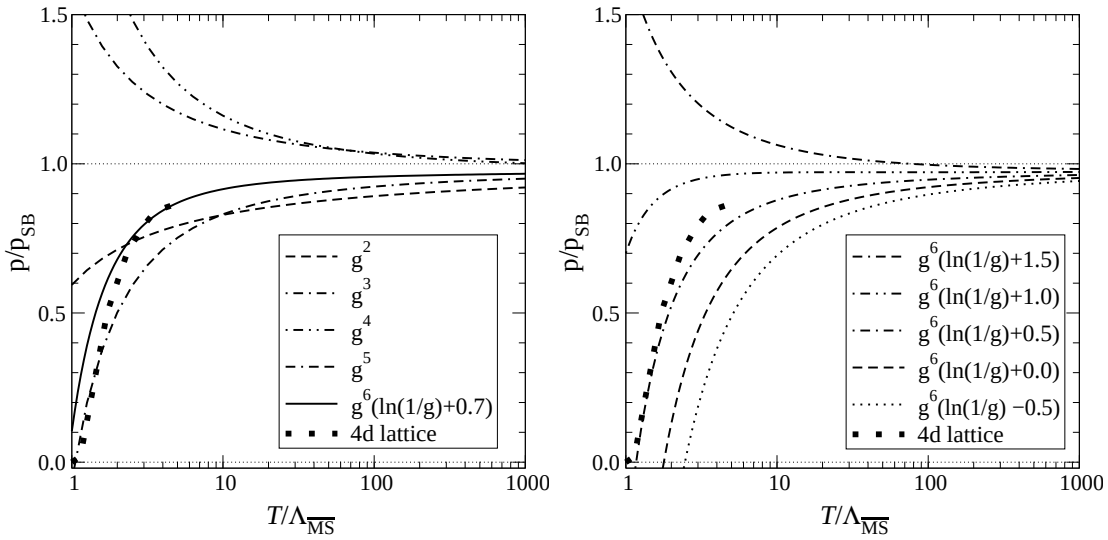

Figure 3.1: Left: perturbative result at various orders in g normalized to the Stefan-Boltzmann value. The $\mathcal{O}(g^6)$ constant has been matched to the 4d lattice results. Right: the effect of varying the still missing g^6 coefficient. The figure is from [36].

three propagators. Hence, in a general graph there are $2l$ vertices and $3l$ propagators. Then a contribution of this type of a diagram to QCD pressure is

$$\sim g^{2l}(2\pi T)^{l+1}\left(\int \mathrm{d}^3p\right)^{l+1}\frac{p^{2l}}{(p^2+m(T)^2)^{3l}}. \tag{3.4}$$

The $m(T)$ is a static infrared cutoff, which appears due to high temperature effects. In the case $l > 3$ the result of the loop integral (3.4) is of the form

$$\sim g^6T^4\left(\frac{g^2T}{m(T)}\right)^{l-3}, \tag{3.5}$$

which can be seen, e.g., by dimensional grounds. The problem becomes apparent when one inspects the infrared sensitive modes $m \sim g^2T$ (see the next section for more discussion about the scales in the theory). Then all loops with $l > 3$ contribute to the term of order g^6. Because no method of summing all of these infinite numbers of loop orders has been found, it is apparent that a different approach is needed. Even if at extremely high temperatures $T > 1000T_\mathrm{c}$ the effect of g^6 term is negligible, its contribution at lower temperatures might still be significant. Especially, it is the first non-perturbative coefficient, and therefore its size might differ significantly from the already known coefficients. Additionally, it is possible that if the effect of the g^6 term is taken into account, the perturbation theory might be applicable to surprisingly low temperatures [36], see also Fig. 3.1.

One approach is to perform full QCD lattice simulations and to fit the order g^6 coefficient. However, the simulations should be performed at extremely high temperature in order to obtain a well controlled difference between perturbation theory and lattice calculations. On top of that, the pressure is an exceptionally demanding quantity to calculate using lattice simulations. The simulation parameters must fulfill a wide range of conditions

$$a \ll \frac{1}{T} \ll \frac{1}{T_\mathrm{c}} \ll L. \tag{3.6}$$

In addition, one has to somehow normalize the zero-point energy. This is achieved by subtracting the zero-temperature result from the corresponding finite-temperature results. The difference is particularly difficult to evaluate because both terms being subtracted contain an unphysical contribution that scales approximately $1/(aT)^4$. Hence, as the continuum limit is approached, the numerical signal decreases rapidly [18]. This renders the finite temperature simulations in practice impossible in the region where perturbation theory would be applicable. Therefore, a novel approach is needed.

3.2 Dimensional reduction

A solution to the problem of the calculation of the order g^6 coefficient is to use the same method than in most recent perturbative computations, namely dimensional reduction. It was first developed the in early 1980's by Ginsparg, and Appelquist and Pisarki [37, 38]. Since then it has been widely used as a method to gain insight into the qualitative behavior of field theories at high temperature [39, 40]. But after the works by Farakos, Kajantie, Rummukainen, and Shaposhnikov [41, 42], who applied it to the electroweak phase transition, and Braaten and Nieto, who applied it to a scalar field with ϕ^4 interactions [43], it has proven also to be an effective method for quantitative calculations both in perturbation theory [32, 44, 45, 46, 47, 48] and lattice simulations [49, 50, 51]. Braaten and Nieto also first presented the procedure, how to evade the infrared problems of QCD [25].

The basic idea of dimensional reduction becomes apparent from the Fourier decomposition of the fields (2.10). One discovers that 4d finite-temperature field theory is exactly equivalent to a 3d zero-temperature theory with an infinite number of fields. Substituting the fields into the QCD Lagrangian[2], (2.12) the 3d fields acquire a correction to their masses. The masses of bosons are $m_{\mathrm{B}} = 2\pi nT$ and those of the fermions $m_{\mathrm{F}} = \pi T(2n+1)$, where $n \geq 0$ is an integer. Hence, all the fermionic modes and the dynamic bosonic modes ($n \neq 0$) have an effective mass proportional to $\sim \pi T$. Therefore, if we are interested in infrared physics only, one naturally expects the heavy modes to decouple.

The naive approach is to discard the fermions and heavy bosonic modes and write

$$\int \mathrm{d}^4x \frac{1}{4} F^a_{\mu\nu} F^{\mu\nu}_a \to \frac{1}{T} \int \mathrm{d}^3x \left\{ \frac{1}{2} \mathrm{Tr} F^2_{kl} + \mathrm{Tr}[D_k, A_0] \right\}, \tag{3.7}$$

where $F^a_{ij} = \partial_i A^a_j - \partial_j A^a_i + g_{\mathrm{E}} f^{abc} A^b_i A^c_i$, $D_k = \partial_k - i g_{\mathrm{E}} A_k$, and we have used the shorthand notation $A_k = A^a_k T^a$, $A_0 = A^a_0 T^a$. However, as pointed out by Landsman (in contrast to zero temperature theory [52]), this kind of complete decoupling does not occur at limit $T \to \infty$ [40]. Rather, the non-static modes generate an infinite number of effective vertices for the static modes which cannot in general be ignored.

The method is to write down the most general 3d Lagrangian for the static modes, which includes all the operators up to the required order. The resulting theory needed to calculate the

[2]This holds for any lagrangian with a quadratic kinetic part.

pressure up to order g^6 is called EQCD which we define by

$$\begin{aligned} p_{\rm QCD} &\equiv p_{\rm E} + \frac{T}{V}\ln\int \mathcal{D}A_k^a \mathcal{D}A_0^a \exp(-S_{\rm E}), \\ S_{\rm E} &= \int \mathrm{d}^d x \mathcal{L}_{\rm E}, \\ \mathcal{L}_{\rm E} &= \frac{1}{2}{\rm Tr}F_{kl}^2 + {\rm Tr}[D_k, A_0]^2 + m_{\rm E}^2 {\rm Tr}A_0^2 \\ &\quad + i\gamma_{\rm E}{\rm Tr}A_0^3 + \lambda_{\rm E}^{(1)}({\rm Tr}A_0^2)^2 + \lambda_{\rm E}^{(2)}{\rm Tr}A_0^4 + \ldots . \end{aligned} \tag{3.8}$$

In addition to the operators shown explicitly, there are also higher order ones, which start to contribute from order $\mathcal{O}(T^3 g^7)$. The lowest such operators have been listed in [53].

We use dimensional regularisation in order to regulate the ultraviolet divergences appearing in the perturbative matching. We write the momentum integration measure as

$$\int \frac{\mathrm{d}^d p}{(2\pi)^d} = \Lambda^{-2\epsilon}\left[\left(\frac{e^\gamma \bar{\Lambda}^2}{4\pi}\right)^\epsilon \int \frac{\mathrm{d}^d p}{(2\pi)^d}\right], \tag{3.9}$$

where $\bar{\Lambda} \equiv (4\pi e^{-\gamma})^{1/2}\Lambda$ is the scale parameter of $\overline{\rm MS}$ renormalization scheme and γ is the Euler-Mascheroni constant. The factor $\Lambda^{-2\epsilon}$ is suppressed since we are only interested in quantities that are finite in the limit $\epsilon \to 0$. We use the notation of [54] and denote the scale with Λ instead of the more common choice μ to distinguish it from the chemical potential.

One notable property of EQCD is that it is superrenormalizable. This makes it much easier to analyze with perturbative and non-perturbative methods. In contrast to the 4d theory, where ultraviolet divergences exist at any order of perturbation theory, in 3d only 1- and 2-loop graphs are divergent. This enables us also to convert the lattice measurements exactly to the continuum using lattice perturbation theory, see Appendix A.

On the downside, EQCD cannot describe the QCD phase transition since at too low T the QCD coupling becomes strong and the perturbative derivation of EQCD fails. Nevertheless, the theory has been observed to be quantitatively accurate down to surprisingly low temperatures of order 1.5-4 $T_{\rm c}$, depending on the quantity of interest.

In the relation of Eq. (3.8) there appear six different matching coefficients, $p_{\rm E}$, $m_{\rm E}^2$, $g_{\rm E}^2$, $\gamma_{\rm E}$, $\lambda_{\rm E}^{(1)}$, and $\lambda_{\rm E}^{(2)}$. The $p_{\rm E}$ contains contributions to the pressure from the hard scales $\sim \pi T$ and is fully perturbative. The other matching coefficients are determined by requiring that EQCD reproduces the same static gauge-invariant correlation functions than full QCD at distances $L \gg 1/T$. The coefficients have to be calculated up to sufficient depth to obtain the pressure

up to order $\mathcal{O}(g^6)$. The quantities written to the required order read:

$$\begin{aligned}
p_{\rm E} &= T^4\left[\alpha_{\rm E1}+g^2\big(\alpha_{\rm E2}+\mathcal{O}(\epsilon)\big)+\right.\\
&\qquad\left.+\frac{g^4}{(4\pi)^2}\big(\alpha_{\rm E3}+\mathcal{O}(\epsilon)\big)+\frac{g^6}{(4\pi)^4}\big(\beta_{\rm E1}+\mathcal{O}(\epsilon)\big)+\mathcal{O}\left(g^8\right)\right] && (3.10)\\
m_{\rm E}^2 &= T^2\left[g^2\left(\alpha_{\rm E4}+\alpha_{\rm E5}\epsilon+\mathcal{O}\left(\epsilon^2\right)\right)+\frac{g^4}{(4\pi)^2}\big(\alpha_{\rm E6}+\beta_{\rm E2}\epsilon+\mathcal{O}(\epsilon)\big)\right] && (3.11)\\
g_{\rm E}^2 &= T\left[g^2+\frac{g^4}{(4\pi)^2}\left(\alpha_{\rm E7}+\beta_{E3}\epsilon+\mathcal{O}\left(\epsilon^2\right)\right)\right] && (3.12)\\
\lambda_{\rm E}^{(1)} &= T\frac{g^4}{(4\pi)^2}\left(\beta_{\rm E4}+\mathcal{O}(\epsilon)\right) && (3.13)\\
\lambda_{\rm E}^{(2)} &= T\frac{g^4}{(4\pi)^2}\left(\beta_{\rm E5}+\mathcal{O}(\epsilon)\right) && (3.14)\\
\gamma_{\rm E} &= \frac{g^3}{3\pi^2}\sum_f \mu_f && (3.15)
\end{aligned}$$

where coefficient $\alpha_{\rm E4}$, $\alpha_{\rm E6}$, $\alpha_{\rm E7}$, $\beta_{\rm E5}$, and $\beta_{\rm E5}$, which in the general case depend on the chemical potential μ, are known and given in [50, 55][3]. The $\beta_{\rm E1}\ldots\beta_{\rm E3}$ are still unknown coefficients, but well-defined and purely perturbative. At $\mu=0$ also $\beta_{\rm E2}$ and $\beta_{\rm E3}$ are known [48]. The determination of $\beta_{\rm E1}$ requires a calculation of the four-loop vacuum integrals of the theory amounting to the computation of about 25×10^6 sum-integrals, which can be considered a challenging task. However, lately some progress has been made and the first non-trivial integral has been successful calculated [56].

Note that at finite chemical potential the action is complex. Hence, as finite density QCD, also EQCD suffers from the sign problem. This will be discussed in more detail in forthcoming chapters. Observe also that when $N_{\rm c}=2,3$, the two quartic operators in Eg. (3.8) are related through

$$(\mathrm{Tr}[A_0^2])^2 = 2\mathrm{Tr}[A_0^4]. \tag{3.16}$$

For future use we define the following dimensionless ratios

$$\begin{aligned}
x &\equiv \frac{\lambda_{\rm E}^{(1)}}{g_{\rm E}^2} && (3.17)\\
y &\equiv \frac{m_{\rm E}^2}{g_{\rm E}^4} && (3.18)\\
z &\equiv \frac{\gamma_{\rm E}}{g_{\rm E}^3}. && (3.19)
\end{aligned}$$

[3]Note the different definition of $\bar{\mu}$ in [55]

The dimensionless couplings can be written using the physical variables for $N_{\rm c}=3$ as follows

$$g_{\rm E}^2 = \frac{24\pi^2}{33-2N_{\rm f}}\frac{T}{\bar{\Lambda}_g/\Lambda_{\overline{\rm MS}}}\left(1-\sum_{i=1}^{N_{\rm f}}\frac{1}{9-N_{\rm f}}\mathcal{D}(\bar{\mu}_i)x+\mathcal{O}(x^2)\right) \tag{3.20}$$

$$x = \frac{9-N_{\rm f}}{33-2N_{\rm f}}\frac{1}{\bar{\Lambda}_x/\Lambda_{\overline{\rm MS}}}\left(1-\sum_{i=1}^{N_{\rm f}}\frac{1}{9-N_{\rm f}}\mathcal{D}(\bar{\mu}_i)x+\mathcal{O}(x^2)\right) \tag{3.21}$$

$$\begin{aligned} y = {} & \frac{(9-N_{\rm f})(6+N_{\rm f})}{144\pi^2 x}\left(1+\sum_{i=1}^{N_{\rm f}}\frac{3}{6+N_{\rm f}}\bar{\mu}_i^2\right)+ \\ & \frac{486-33N_{\rm f}-11N_{\rm f}^2-2N_{\rm f}^3}{96\pi^2(9-N_{\rm f})}\left(1+\sum_{i=1}^{N_{\rm f}}\frac{3(7+N_{\rm f})(9-2N_{\rm f})}{486-33N_{\rm f}-11N_{\rm f}^2-2N_{\rm f}^3}\bar{\mu}_i^2\right)+\mathcal{O}(x) \end{aligned} \tag{3.22}$$

$$z = \sum_{i=1}^{N_{\rm f}}\frac{\bar{\mu}_i}{3\pi}\left(1+\frac{21+3N_{\rm f}}{18-2N_{\rm f}}x\right)+\mathcal{O}(x^2), \tag{3.23}$$

where $\bar{\mu}=\mu/(\pi T)$, and, for small $\bar{\mu}$, $\mathcal{D}(\bar{\mu})\approx -7\zeta(3)\bar{\mu}^2/2$, and

$$\bar{\Lambda}_g = 4\pi T\exp\left(\frac{-3+4N_{\rm f}\log 4}{66-4N_{\rm f}}-\gamma_{\rm E}\right), \tag{3.24}$$

$$\bar{\Lambda}_x = 4\pi T\exp\left(\frac{-162+102N_{\rm f}-4N_{\rm f}^2+(36N_{\rm f}-4N_{\rm f}^2)\log(4)}{594-75N_{\rm f}+N_{\rm f}^2}-\gamma_{\rm E}\right). \tag{3.25}$$

The equation (3.22) defines a "constant physics curve" within EQCD, from the point of view of full 4d QCD.

As can be seen from the equations (3.11)-(3.15) there are still two different scales gT and g^2T in this theory. The procedure can be continued by integrating out the field A_0. This field accounts for the effects of the color-electric scale gT. The resulting theory is called magnetostatic QCD (MQCD) and reads

$$\begin{aligned} \frac{T}{V}\ln\int\mathcal{D}A_k^a\mathcal{D}A_0^a\exp(-S_{\rm E}) &\equiv p_{\rm M}+\frac{T}{V}\ln\int\mathcal{D}A_k^a\exp(-S_{\rm M}), \\ S_{\rm M} &= \int{\rm d}^dx\mathcal{L}_{\rm M}, \\ \mathcal{L}_{\rm M} &= \frac{1}{2}{\rm Tr}F_{kl}^2+\ldots, \end{aligned} \tag{3.26}$$

where $F_{kl}=i/g_{\rm M}[D_k,D_k]$, $D_k=\partial_k-ig_{\rm M}A_k$. Again there are higher order corrections to the Lagrangian $\mathcal{L}_{\rm M}$, but they would contribute to the pressure only at order $\mathcal{O}(T^3g^9)$. The two

matching coefficients $p_{\rm M}$ and $g_{\rm M}$ of MQCD, given to the required depth, are

$$\begin{aligned}
\frac{p_{\rm M}}{T} &= \frac{1}{(4\pi)} m_{\rm E}^3 \left[\frac{1}{3} + \mathcal{O}(\epsilon)\right] \\
&+ \frac{1}{(4\pi)^2} d_{\rm A} C_{\rm A} g_{\rm E}^2 m_{\rm E}^2 \left[-\frac{1}{4\epsilon} - \frac{3}{4} - \ln\frac{\bar{\Lambda}}{2m_{\rm E}} + \mathcal{O}(\epsilon)\right] \\
&+ \frac{1}{(4\pi)^3} d_{\rm A} C_{\rm A}^2 g_{\rm E}^4 m_{\rm E} \left[-\frac{89}{24} - \frac{\pi^2}{6} + \frac{11}{6}\ln 2 + \mathcal{O}(\epsilon)\right] \\
&+ \frac{1}{(4\pi)^4} d_{\rm A} C_{\rm A}^3 g_{\rm E}^6 \left[\alpha_{\rm M1}\left(\frac{1}{\epsilon} + 8\ln\frac{\bar{\Lambda}}{2m_{\rm E}}\right) + \beta_{M1} + \mathcal{O}(\epsilon)\right] \\
&+ \frac{1}{(4\pi)^2} d_{\rm A}(d_{\rm A}+2)\lambda_{\rm E}^{(1)} m_{\rm E}^2 \left[-\frac{1}{4}\right] \\
&+ \frac{1}{(4\pi)^2} \frac{d_{\rm A}(2d_{\rm A}-1)}{N_{\rm c}} \lambda_{\rm E}^{(2)} m_{\rm E}^2 \left[-\frac{1}{4} + \mathcal{O}(\epsilon)\right] \\
&+ \frac{1}{(4\pi)^4} d_{\rm A} D T_{\rm f}^2 g_{\rm E}^6 \left(\frac{1}{2N_{\rm f}}\sum_f \bar{\mu}\right)^2 \left[\alpha_{\rm M2}\left(\frac{1}{\epsilon} + 4\ln\frac{\bar{\Lambda}}{2m_{\rm E}}\right) + \beta_{\rm M2} + \mathcal{O}(\epsilon)\right], \qquad (3.27) \\
g_{\rm M}^2 &= g_{\rm E}^2 + \mathcal{O}\left(g^3\right), \qquad (3.28)
\end{aligned}$$

where $\bar{\mu} = \mu/(\pi T)$ and the group theoretical factors included in the expression are

$$\begin{aligned}
C_{\rm A}\delta^{cd} &\equiv f^{abc}f^{abd} = N_{\rm c}\delta^{cd} && (3.29)\\
C_{\rm F}\delta_{ij} &\equiv (T^aT^a)_{ij} = \frac{N_{\rm c}^2-1}{N_{\rm c}}\delta_{ij} && (3.30)\\
T_{\rm f}\delta^{ab} &\equiv {\rm Tr}T^aT^b = \frac{N_{\rm f}}{2}\delta^{ab} && (3.31)\\
D\delta^{cd} &\equiv d^{abc}d^{abd} = \frac{N_{\rm c}^2-4}{N_{\rm c}}\delta^{cd} && (3.32)\\
d_{\rm A} &\equiv \delta^{aa} = N_{\rm c}^2 - 1 && (3.33)\\
d_{\rm F} &\equiv \delta^{ii} = \frac{d_{\rm A}T_{\rm f}}{C_{\rm F}} = N_{\rm c}N_{\rm f}, && (3.34)
\end{aligned}$$

where the trace of Eq. (3.31) is taken over both color and flavor indices.

After the second reduction step we are left with the contribution from MQCD

$$p_{\rm G} \equiv \frac{T}{V}\int \mathcal{D}A_k^a \exp(-S_{\rm M}). \qquad (3.35)$$

The theory has only one parameter $g_{\rm M}$ with a dimension of ${\rm GeV}^{1/2}$. Because there are no mass scales in the propagator, the perturbation theory result of the pressure in dimensional regularisation scheme erroneously vanishes. The calculation of the pressure results in an expression with divergences from both IR and UV, which cancel each other exactly. However, the pressure having a dimension of ${\rm GeV}^4$ the non-perturbative contribution must be of the form

$$\frac{p_{\rm G}}{T} = g_3^6\left[A'_G \ln\frac{\bar{\mu}}{g_3^2} + B'_G\right]. \qquad (3.36)$$

The coefficient of the logarithm has been calculated by introducing a mass-scale $m_{\rm G}^2$ for the gauge and ghost field propagators and sending $m_{\rm G}^2 \to 0$ after the calculation. The result in the $\overline{\rm MS}$ scheme, which regulates away the $1/\epsilon$ divergences, reads

$$\frac{p_{\rm G,\overline{MS}}}{T} = g_3^6 \frac{d_A N_{\rm c}^3}{(4\pi)^4} \left[\left(\frac{43}{12} - \frac{157}{768}\pi^2 \right) \ln \frac{\bar{\mu}}{2N_{\rm c} g_3^2} + B_{\rm G}(N_{\rm c}) + \mathcal{O}(\epsilon) \right]. \tag{3.37}$$

The procedure naturally breaks the gauge symmetry of Eq. (2.14), so in a perturbative framework the quantity $B_{\rm G}(N_{\rm c})$ is unphysical. To compute $B_{\rm G}(N_{\rm c})$ non-perturbatively, which in general is a function of $N_{\rm c}$, we have to perform lattice simulations. Because of the superrenormalizability of the theory, the result can be converted exactly to the $\overline{\rm MS}$ scheme.

3.3 Validity of dimensional reduction

An important question is when the dimensional reduction approach is reliable. Formally, the error in the dimensional reduction procedure can be parametrized as [42]

$$(V_4 - TV_3)/T^4 = \mathcal{O}(m_i^2(T)/T^2), \tag{3.38}$$

where V_4 and V_3 are effective potentials computed in QCD and EQCD respectively. The $m_i(T)$ are the relevant mass scales of the system, i.e., inverse screening and correlation lengths, which at high temperatures are proportional to $\sim gT$. Hence, a formal requirement of the validity of dimensional reduction is the same than that for $T = 0$ perturbation theory $g^2 \ll 1$.

It is important to note that the criterion is not same as the one for finite T perturbation theory, which is valid down to energy scales $Q \sim g^2 T$, where Q is a typical energy scale which is much smaller than the temperature. Hence, there is a parameter range where finite temperature perturbation theory does not hold,

$$\frac{g^2 T}{Q} \geq 1, \tag{3.39}$$

but dimensional reduction works as $g^2 \ll 1$. Hence, lattice simulations of EQCD do not only provide corrections to the weak coupling expansion, but also extend the results down to temperatures where perturbation theory is not valid.

Therefore, it is understandable that EQCD provides reliable results down to temperatures as low as $T \sim 2 - 4T_{\rm c}$, depending on the quantity of interest. Especially good results have been obtained in the calculation of static correlation lengths [50]. An interesting study of the validity of dimensional reduction has been conducted in [57], where the authors study the symmetry group of the spatial transfer matrix by measuring the screening masses. They find out that the spectrum obtained from 4d QCD corresponds to that expected from dimensionally reduced theory already at $T \sim 2T_{\rm c}$. The other limiting case for the validity of EQCD is the limit of large μ, which has been studied in [58]. It is found out that EQCD is valid for arbitrary high μ/T as long as πT is larger than the scales in EQCD, namely $\pi T \gtrsim m_{\rm E}$.

Unfortunately, the dimensional reduction, in the case of QCD, cannot be extended to include the properties of the deconfinement phase transition[4]. However, the EQCD has a non-trivial phase diagram with some resemblances to the QCD one. QCD without matter possess a $Z(3)$

[4] In contrast, the phase transition of the electroweak theory can be studied in the framework of dimensional reduction [41, 42].

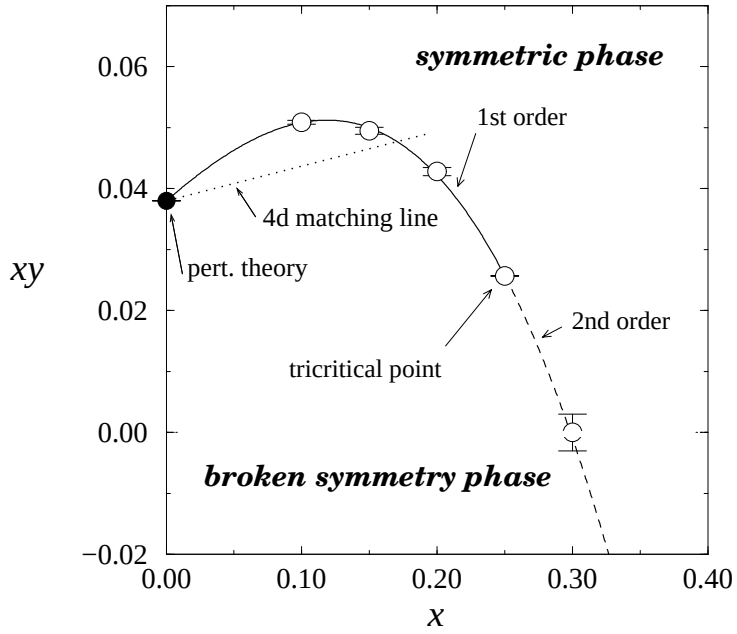

Figure 3.2: The EQCD phase diagram with the dimensionless variables x and y. The temperature decreases from left to right. The solid line represents the first-order phase transition line, which changes to second order at the tricritical point. The dotted line is the "constant physics" curve. The figure is from [59].

symmetry, which is spontaneously broken in the high temperature phase. The order parameter is the Polyakov loop $L(\mathbf{x})$

$$L(\mathbf{x}) = \frac{1}{N_\mathrm{c}} \mathrm{Tr} P \exp\left[ig \int_0^\beta \mathrm{d}\tau A_0(\tau, \mathbf{x}) \right]. \tag{3.40}$$

In the broken phase, it has an expectation value $\sim e^{i2\pi k/N_\mathrm{c}}$, where k is an integer. One can define a transformation of the fields, so that the action is invariant but $L \to e^{i2\pi k/N_\mathrm{c}} L$.

On the other hand EQCD has also 3 different phases: a symmetric $\langle \hat{A}_0^3 \rangle = 0$ and 2 broken phases with non-zero $\langle \hat{A}_0^3 \rangle$ related by the reflection $\langle \hat{A}_0^3 \rangle \leftrightarrow -\langle \hat{A}_0^3 \rangle$ [60] (see also [61]). However, the construction of EQCD requires small amplitudes of the adjoint field A_0, $A_0 \ll 2\pi T/g$, which means that to describe QCD properly, EQCD must stay on the symmetric A_0-phase, and the Z(3) invariance of QCD is broken in EQCD. Discouragingly, the "constant physics curve" (3.22), which corresponds to the physical 4d values of the parameters lies inside the broken phase $\langle \hat{A}_0^3 \rangle \neq 0$. However, the phase transition is strongly first order for physically relevant parameter values, which guarantees that the theory is metastable, enabling us to perform meaningful simulations in EQCD. At higher values of x there is a tricritical point, after which the phase transition is of second order. Interestingly, the tricritical point lies close to the physical QCD phase transition, see Fig. 3.2.

There are also a promising constructions of dimensionally reduced effective theories, which possess the correct $Z(N_\mathrm{c})$-symmetry. A Z(3) invariant theory is described in [59] and studied on

lattice in [62, 63], and a corresponding Z(2) theory is constructed in [64]. It is hoped that the correct symmetry structure of the effective theories would improve the behaviour of the theory near T_c compared to EQCD. However, quantitative calculations of physical observables are still missing, and therefore it is unclear if these theories describe the physics close to phase transition any better than EQCD.

Chapter 4

Calculations of $B_{\mathrm{G}}(N_{\mathrm{c}})$

Next we will describe the computation of non-perturbative input $B_{\mathrm{G}}(N_{\mathrm{c}})$ to the pressure. We will carry out lattice measurements with $N_{\mathrm{c}} = 2$, 3, 4, 5 and 8 to obtain N_{c}-dependence of the non-perturbative input to pressure. This gives us an independent check for the physical $N_{\mathrm{c}} = 3$ case and acts as a consistency check for the entire pressure calculation. Namely, we expect to see a smooth behavior of the observable in N_{c}. Additionally, there are various other physical motivations to study the N_{c}-dependence and especially the large-N_{c} limit of SU(N_{c}) gauge theories [65]. The limit $N_{\mathrm{c}} \to \infty$ simplifies the theory significantly, but nevertheless the phenomenology is in many ways similar to SU(3). These reasons have motivated numerous large-N_{c} limit studies on the lattice [66, 67, 68].

We start the chapter by formulating EQCD on the lattice. We also discuss the relation between $B_{\mathrm{G}}(N_{\mathrm{c}})$ and the lattice observables. The main part of the chapter is devoted to the technicalities of the lattice simulations. At the end we also describe, how the reliability of the result can be tested.

4.1 EQCD on the lattice

For the the calculation of $B_{\mathrm{G}}(N_{\mathrm{c}})$ only the lattice simulations of MQCD are needed. However, for later use we will introduce entire EQCD on the lattice. We introduce a three-dimensional spatial lattice with a lattice spacing a. Every point on the lattice is then specified by three integers $\mathbf{n} \equiv (n_1, n_2, n_3)$. Hence, the adjoint Higgs field can be written on the lattice as

$$\begin{aligned} x_k &\to n_k a \\ A_0(\mathbf{x}) &\to A_0(\mathbf{n}a) \\ \int \mathrm{d}^3x &\to a^3 \sum_n . \end{aligned} \tag{4.1}$$

To keep the notation simple, we will still denote the position with x, but in the case of the lattice, it has to be considered a discrete variable.

The gauge field part of the action can be obtained as suggested by Wilson [13] defining link matrices U_k through

$$\begin{aligned} U_i &= P \exp\left[i g_{\mathrm{E}} \int_x^{x+k} \mathrm{d}x_k A_k \right] \\ &= \exp\left[i g_{\mathrm{E}} a A_k(x) \right]. \end{aligned} \tag{4.2}$$

The link matrices U_k act as a parallel transporters from one lattice site to a neighbouring one. They transform in a gauge transformation $\Lambda \in \mathrm{SU}(N_\mathrm{c})$ as

$$U_k(x) \rightarrow \Lambda(x)U_i(x)\Lambda^\dagger(x+\hat{k}) \tag{4.3}$$
$$U_k^\dagger(x) \rightarrow \Lambda(x+\hat{k})U_i(x)^\dagger\Lambda^\dagger(x), \tag{4.4}$$

where $\hat{k}$ is a unit vector to direction k. In the limit of $a \to 0$, this expression reduces to (2.14). It is obvious that the only gauge invariant quantities containing link matrices only are traces of closed loops. The simplest closed loop is the *plaquette*

$$P_{kl}(x) = \left[U_k(x)U_l(x+\hat{k})U_k^\dagger(x+\hat{l})U_l^\dagger(x)\right]. \tag{4.5}$$

Expanding in a, the plaquette reduces to

$$\mathrm{ReTr}P_{kl}(x) = N_\mathrm{c}\left[1 - \frac{a^4 g^2}{4}F_{kl}^a F_{kl}^a + \mathcal{O}\left(g_\mathrm{E}^4 a^6\right)\right]. \tag{4.6}$$

On the lattice the adjoint A_0 field transforms in the gauge transformation as

$$A_0(x) \rightarrow \Lambda(x)A_0(x)\Lambda^\dagger(x). \tag{4.7}$$

With adjoint fields A_0 and gauge fields U, the "string" type of quantities are also gauge invariant. The simplest being

$$\mathrm{Tr}[A_0(x)U_k(x)A_0(\mathbf{x}+\hat{k})U_k^\dagger(\mathbf{x})], \tag{4.8}$$

which reduces in the continuum limit to

$$\mathrm{Tr}[A_0^2] - \frac{a^2}{2}\mathrm{Tr}[D_k, A_0]^2 + \mathcal{O}\left(g_\mathrm{E}^2 a^4\right). \tag{4.9}$$

Hence, we can write the EQCD action on the lattice as a

$$S_a = S_a^\mathrm{YM} + S_a^\mathrm{AH}, \tag{4.10}$$
$$S_a^\mathrm{YM} = \beta\sum_\mathbf{x}\sum_{k<l}\left(1 - \frac{1}{N_\mathrm{c}}\mathrm{ReTr}[P_{kl}(\mathbf{x})]\right) \tag{4.11}$$
$$S_a^\mathrm{AH} = 2a\sum_\mathbf{x}\sum_k\left(\mathrm{Tr}[A_0^2(\mathbf{x})] - \mathrm{Tr}[A_0(\mathbf{x})U_k(\mathbf{x})A_0(\mathbf{x}+\hat{k})U_k^\dagger(\mathbf{x})]\right) \tag{4.12}$$
$$+a^3\sum_\mathbf{x}\left(m_\mathrm{bare}^2\mathrm{Tr}A_0^2(\mathbf{x}) + i\gamma_\mathrm{E}\mathrm{Tr}[A_0^3(\mathbf{x})] + \lambda_\mathrm{E}(\mathrm{Tr}[A_0^2(\mathbf{x})])^2\right), \tag{4.13}$$

where $\beta = \frac{2N_\mathrm{c}}{ag_\mathrm{E}^2}$ and m_bare^2 is a bare mass parameter that has to be renormalized before simulations. Other couplings do not need renormalization. Note also that because we are going to perform the EQCD simulations at $N_\mathrm{c} = 3$, we have set $\lambda_\mathrm{E}^{(2)} = 0$, and denote $\lambda_\mathrm{E} \equiv \lambda_\mathrm{E}^{(1)}$. The MQCD action on lattice is S_a^YM.

The lattice action reproduces the continuum action in the formal continuum limit $a \to 0$ or $\beta \to \infty$, but includes corrections of $\mathcal{O}(a)$. One can naturally introduce improvements which disappear in the continuum limit but cancel the effects at $\mathcal{O}(a)$. Some improvements for the coupling λ_E and mass parameter m_E have been calculated in [69]. We will, however, not implement them, because in simulations of EQCD they have been found irrelevant.

To perform the actual computer simulations, we follow the implementation of [61] and write the action as

$$\begin{aligned} S_{latt} &= \beta \sum_{\mathbf{X}} \sum_{k<l} \left(1 - \frac{1}{N_{\rm c}} {\rm ReTr}[P_{lk}(\mathbf{x})] \right) \\ &\quad - \frac{4N_{\rm c}}{\beta} \sum_{\mathbf{x},k} {\rm Tr}[\hat{A}_0(\mathbf{x}) U_k(\mathbf{x}) \hat{A}_0(\mathbf{x}+\hat{k}) U_k^\dagger(\mathbf{x})] \\ &\quad + \sum_x \left(\alpha {\rm Tr}[\hat{A}_0^2(\mathbf{x})] + \frac{8N_{\rm c}^3}{\beta^3} iz {\rm Tr}[\hat{A}_0^3(\mathbf{x})] + \frac{8N_{\rm c}^3}{\beta^3} x ({\rm Tr}[\hat{A}_0^2(\mathbf{x})])^2 \right), \end{aligned} \tag{4.14}$$

where $\hat{A}_0 \equiv A_0/g_{\rm E}$. Choosing the scale $\bar{\Lambda} = g_3^2$, the relation between the lattice and continuum mass parameters reads

$$\begin{aligned} \alpha &= \frac{12N_{\rm c}}{\beta} + \frac{8N_{\rm c}^3}{\beta^3} - [2C_{\rm A} + (d_{\rm A}+2)x] \frac{N_{\rm c}\Sigma}{2\pi\beta} \\ &\quad + \frac{N_{\rm c}^2}{4\pi^2\beta^2} \left\{ 2x(d_{\rm A}+2)(x - C_{\rm A})(\left(\ln \frac{3}{N_{\rm c}\beta} + \zeta \right) - 2C_{\rm A} x (d_{\rm A}+2) \left(\frac{\Sigma^2}{4} - \delta \right) \right. \\ &\quad \left. - C_{\rm A}^2 \left[\frac{5}{8}\Sigma^2 + \left(\frac{1}{2} - \frac{4}{3C_{\rm A}^2} \right) \pi\Sigma - 4(\delta+\rho) + 2\kappa_1 - \kappa_4 \right] \right\}, \end{aligned} \tag{4.15}$$

where the lattice constants are given in Appendix A.

4.2 Lattice $\overline{\rm MS}$ relation for $B_G(N_c)$

To obtain $B_{\rm G}(N_{\rm c})$ in the continuum theory, we need to derive the relation between the quantities we can measure in the lattice simulations and $B_{\rm G}(N_{\rm c})$. We begin this by studying the lattice vacuum energy density

$$\frac{p_{\rm G,a}}{T} \equiv -f_a \equiv \ln Z^{\rm YM} = \frac{1}{V} \ln \left[\int \mathcal{D}U_k \, \exp\left(-S_a^{\rm YM} \right) \right]. \tag{4.16}$$

The expression involves an integration over all variables U_k. The $\mathcal{D}U_k$ denotes the so-called Haar measure, which is left and right invariant under the multiplication of group elements of $SU(N_{\rm c})$, depends on $d_{\rm A} = N_c^2 - 1$ real variables parametrizing the elements of ${\rm SU}(N_{\rm c})$, and is of the form

$$\prod_n J(\alpha_n) \prod_{a=1}^{N_c^2-1} {\rm d}\alpha_n^a, \tag{4.17}$$

where α_n^a denote the group parameters of n'th link variable. The structure of the Jacobian $J(\alpha_n)$ is determined from the requirement of gauge invariance.

Because on the lattice there are two dimensionful parameters $g_{\rm E}$ and a, the situation is more complicated than in the continuum. Having a mass dimension ${\rm GeV}^3$ the vacuum energy density can contain terms of the form $g_3^{2n} a^{n-3}$. Thus, in the continuum limit $a \to 0$, we can relate f_a and $f_{\overline{\rm MS}} \equiv -p_{\rm G}/T$ as follows:

$$\Delta f \equiv f_a - f_{\overline{\rm MS}} \tag{4.18}$$

$$= C_1 \frac{1}{a^3} \left(\ln \frac{1}{a g_3^2} + C_1' \right) + C_2 \frac{g_3^2}{a^2} + C_3 \frac{g_3^4}{a} + C_4 g_3^6 \left(\ln \frac{1}{a\bar{\mu}} + C_4' \right) + \mathcal{O}(g_3^8 a). \tag{4.19}$$

Taking derivatives of Eq. (4.18) with respect to g_3^2 and using 3d rotational and translational symmetries on the lattice, we obtain a relation [1, 2]

$$8\frac{d_A N_{\rm c}^6}{(4\pi)^4} B_{\rm G}(N_{\rm c}) = \lim_{\beta\to\infty} \beta^4 \left\{ \langle 1 - \frac{1}{N_{\rm c}} {\rm Tr}[P] \rangle_a - \left[\frac{c_1}{\beta} + \frac{c_2}{\beta^2} + \frac{c_3}{\beta^3} + \frac{c_4}{\beta^4} (\ln\beta + c_4') \right] \right\}. \tag{4.20}$$

Hence, we obtain $B_{\rm G}(N_{\rm c})$ by measuring the plaquette as a function of $N_{\rm c}$ on the lattice. The relations between c_i and C_i read

$$\begin{aligned} c_1 &= C_1/3 & c_2 &= -\frac{2N_{\rm c}}{3} C_2 & c_3 &= -\frac{8N_{\rm c}^2}{3} C_3 \\ c_4 &= -8N_{\rm c}^3 C_4 & c_4' &= C_4' - \frac{1}{3} - 2\ln(2N_{\rm c}). \end{aligned} \tag{4.21}$$

The coefficients c_1-c_3 can be calculated by means of lattice perturbation theory. An outline of the calculation and the numerical values of these parameters are given in Appendix A. Because there is no $\bar{\Lambda}$ dependence in f_a, the c_4 is determined by the $\overline{\rm MS}$ value of the logarithmic coefficient of equation (3.37),

$$c_4 = 8\frac{d_{\rm A} N_{\rm c}^6}{(4\pi)^4} \left(\frac{43}{12} - \frac{157}{768}\pi^2 \right). \tag{4.22}$$

The coefficient c_4' is more problematic since the four-loop free energy itself is an IR divergent quantity in both the $\overline{\rm MS}$ and lattice schemes. But the finite difference between them, c_4', can be defined by introducing the same IR cutoff, e.g., a gluon mass, in both schemes. The cutoff dependence then cancels out when the two schemes are compared. The $\overline{\rm MS}$ result has been calculated in [32], but the lattice counterpart is known only for $N_{\rm c} = 3$, for which it has been calculated using stochastic perturbation theory [70]. The result reads

$$c_4' = 7.0 \pm 0.3. \tag{4.23}$$

For later use, we define a quantity

$$P_G(\beta, N_{\rm c}) \equiv \frac{32\pi^4\beta^4}{d_A N_{\rm c}^6} \left\{ \langle 1 - \frac{1}{N_{\rm c}} {\rm Tr}[P] \rangle_a - \left[\frac{c_1}{\beta} + \frac{c_2}{\beta^2} + \frac{c_3}{\beta^3} + \frac{c_4}{\beta^4} \ln\beta \right] \right\}, \tag{4.24}$$

which is a normalized plaquette expectation value minus all the ultraviolet divergences. Hence,

$$B_{\rm G}(N_{\rm c}) - \left(\frac{43}{12} - \frac{157}{768}\pi^2 \right) c_4' = P_G(\infty, N_{\rm c}). \tag{4.25}$$

The $P_G(\infty, N_c)$ has been determined in [2]. After the $N_{\rm c}$-dependence of c_4' has been determined by, e.g., stochastic perturbation theory, one has reached the final goal, the determination of $B_G(N_c)$.

4.2.1 Large-$N_{\rm c}$ limit

In the large $N_{\rm c}$-limit the theory reduces to the so-called planar diagram theory developed by 't Hooft [65]. The statement is that the limit $N_{\rm c} \to \infty$ and $g_{\rm E} \to 0$, such that $\lambda = g_{\rm E}^2 N_{\rm c}$ is kept fixed, leads to an expansion in λ (called the 't Hooft coupling), for which all the Feynman diagrams are planar. Using the 't Hooft coupling at the planar limit, the P_G can be written as

$$P_G(\lambda_a, \infty) = \frac{512\pi^4}{\lambda_a^4} \left\{ \langle 1 - \frac{1}{N_{\rm c}} {\rm Tr}[P] \rangle_a - \left[\hat{c}_1\lambda_a + \hat{c}_2\lambda_a^2 + \hat{c}_3\lambda_a^3 - \hat{c}_4\lambda_a^4 \log(\lambda_a) \right] \right\}, \tag{4.26}$$

where $\lambda_a = a\lambda$ and the $\hat{c}_i$ are numbers independent of N_c. Because the 't Hooft-coupling provides the leading N_c behaviour, we expect that $P_G(\lambda) = \mathrm{const} + \mathcal{O}\left(1/\mathrm{N_c}\right)$. We also suspect the leading order corrections to be $1/N_\mathrm{c}^2$ since perturbation theory produces only even powers of N_c^2. Naturally, being a non-perturbative quantity the, functional form of $P_G(\lambda, N_\mathrm{c})$ can be different form perturbation theory, especially since there are results from other pure gauge theory observables with corrections of $1/N_\mathrm{c}$ [71].

4.3 Lattice simulations

The details of the lattice computations we have performd have been described in [1, 2]. Here, we will concentrate on simulation algorithms and comment on some interesting results of the simulations.

4.3.1 Simulation algorithms

Because of the huge number of the degrees of freedom in the path integrals, the only known practical method of calculating them numerically are Monte Carlo simulations. Namely, we generate field ensembles with a probability distribution given by the Boltzmann factor $\exp(-S[\phi])$, where ϕ denotes all the fields in the action. Then, the expectation values $\langle O \rangle$ are approximately given by the averages of measurements of independent ensembles

$$\langle O \rangle \approx \frac{1}{N} \sum_{i=1}^{N} O(\{\phi\}_i). \tag{4.27}$$

Hence, the problem is reduced to generating ensembles according to the Boltzmann weight.

Only trivial examples are known where ensembles can be generated from scratch. In all relevant cases, one has to generate an algorithm, which updates an existing ensemble, so that the new ensemble respects the Boltzmann distribution or approaches it if the original one is far off. The process should be independent of the initial ensemble, which must first be updated a sufficiently large number of times, so that equilibrium is reached. The number of steps required for this is called the thermalization time. After the thermalization is completed, one performs a measurement and updates repeatedly until the required precision is achieved. In an ideal case, the measured ensembles would be independent of each other and the errors would decrease as $1/\sqrt{N}$. However, this is rarely the case and the errors behave as

$$\mathrm{Errors} \sim \sqrt{\frac{\tau}{\mathrm{N}}}, \tag{4.28}$$

where the autocorrelation time τ is the number of updates required to make the ensemble independent from the initial ensemble. The autocorrelation time τ depends on the algorithm used, the observables one is studying, and the parameter values of the theory.

The ensembles are usually required to be elements of a Markov chain, which means that the next ensemble depends only on the ensemble preceding it. If $W_f(\phi \to \phi')$ is a transition probability, namely the probability that under an update f an ensemble consisting of fields ϕ is transformed to ϕ', then an update f must fulfill the following properties

1. f must preserve the Boltzmann distribution $p_\mathrm{B}(\phi) \sim \exp(-S[\phi])$

$$\int \mathrm{d}\phi W_f(\phi \to \phi') = p_\mathrm{B}(\phi) \tag{4.29}$$

2. f must be ergodic. This means that, given any configuration, a repeated use of f brings us arbitrary close to any other configuration.

The first requirement is usually hard to prove for any given algorithm. Therefore, one uses a more restrictive condition called detailed balance which reads

$$\frac{W_f(\phi \to \phi')}{W_f(\phi' \to \phi)} = \frac{e^{-S[\phi']}}{e^{-S[\phi]}}. \tag{4.30}$$

The standard algorithms update one link or a site at a time. The first such update algorithm was proposed by Metropolis et al. [72]. One sweeps through the lattice, suggesting a random step for a site. Then, the new value is accepted according to the probability

$$W_f(\phi \to \phi') \sim \begin{cases} \exp\left(-(S[\phi] - S[\phi']\right), & \text{if } \mathrm{S}[\phi] < \mathrm{S}[\phi'] \\ 1 & \text{otherwise} \end{cases} \tag{4.31}$$

This clearly fulfills detailed balance and is ergodic. However, there are more efficient algorithms because the acceptance probability of the Metropolis check (4.31) becomes small when the change suggested is large, which causes longer autocorrelation times.

To update gauge field actions there are two different type of efficient methods: heath bath (HB) and overrelaxation (OR). In the former one a new configuration is generated directly from the probability distribution

$$W_f(\phi \to \phi') \sim \exp(-S[\phi]). \tag{4.32}$$

Hence, the new value is independent of the old value. In the OR algorithm one "reflects" the current state with respect to the action minimum, so that the value of the action does not change. Both algorithms fulfill trivially the requirement of detailed balance, but the OR algorithm is not ergodic and hence must be combined with an ergodic algorithm which usually is HB.

To implement the update algorithms for the gauge field action, we study the local action

$$S_k(\mathbf{x}) = \frac{\beta}{N_\mathrm{c}} \mathrm{ReTr}\left[U_k(\mathbf{x}) X_k(\mathbf{x})\right], \tag{4.33}$$

where X_k is the sum of the neighboring staples defined as

$$X_k(\mathbf{x}) \equiv \sum_{l \neq k} \left[U_l(\mathbf{x} + \hat{k}) U_k^\dagger(\mathbf{x} + \hat{l}) U(\mathbf{x})_l^\dagger + U_l^\dagger(\mathbf{x} + \hat{k} - \hat{l}) U_k^\dagger(\mathbf{x} - \hat{l}) U(\mathbf{x} - \hat{l})_l \right]. \tag{4.34}$$

and U_k is the link to be updated.

Then, in the case of a gauge theory, a heat bath algorithm generates new link matrices U_k from the probability density $P = \exp(-S_k)$. There is an effective algorithm for SU(2) pure gauge theory by Creutz [73], which has been improved for large values of β by Kennedy and Pendleton [74]. For $N_\mathrm{c} > 2$, the updates are usually performed using pseudo HB algorithm, which updates $SU(2)$ subgroups of the $SU(N)$ matrix.[1] The SU(2) is a special case because the sum of SU(2) matrices is proportional to an SU(2) matrix.

For gauge fields, OR update can be performed by finding an matrix $R \in \mathrm{SU(N_c)}$, which minimises the action. Then the state is reflected with respect to the minimum by applying the rotation RU_{old}^{-1} twice to the old link matrix U_{old}. For general SU(N_c), an algorithm was developed by Brown and Woch [76], which also updates the SU(2)-subgroups. However, there

[1] There is also an HB algorithm for SU(3) by Pietarinen [75], but it is unpractical.

is a rather new OR algorithm developed by de Forcrand and Jahn [77][2], which finds a minimum for the the entire link matrix using the singular value decomposition (SVD) $X = U\Sigma V^\dagger$, then $W = UV^\dagger$ minimises the action. However, $\det W \neq 1$ and the matrix must be "projected" to the SU(N_c)-space. The SVD algorithm has considerably smaller autocorrelation times than the one updating the SU(2)-subgroups only.

In the simulations of the plaquette, we performed one Kennedy-Pendleton HB update for one SVD OR update. The number of updated subgroups in HB for $N_\mathrm{c} = 3$, 4, 5, and 8 were 3, 4, 8, and 24, respectively. The subgroups were chosen randomly. After each cycle, we measured the plaquette expectation value. Autocorrelation times were around 0.75. For SU(2), we used a dedicated HB and OR algorithm with same ratio of updates. The autocorrelation time was slightly better: 0.6.

4.3.2 The simulations

A common challenge in lattice simulations is to perform the simulations in a physically relevant parameter range. In MQCD simulations, we have two limitations to concern, namely the effects of finite volume and finite lattice spacing. Because there is a mass gap in the theory, we expect the finite volume effects to be exponentially suppressed in high enough volumes [79]. The quantities characterising the finite volume effects are the longest correlation lengths. They are expected to be proportional to the inverse mass of the lightest glueball (the lightest mass scale in theory), which by dimensional grounds is $\sim g_\mathrm{E}^2$. In Fig. 4.1, we have plotted $P_G(\beta, N_\mathrm{c})$, with different values of N_c and a constant β as a function of $\beta/(NN_\mathrm{c}^2)$. We note that the reduction of the number of lattice points N starts to effect the values of P_G around $\beta/(NN_\mathrm{c}^2) = 0.2$. The scaling in N_c is valid in our parameter range $N_\mathrm{c} = 2 \ldots 8$, indicating that the mass of the glueball behaves to leading order in N_c as $m_\mathrm{gb} \sim N_\mathrm{c} g_3^2$. This behaviour of the mass of the glueball is also confirmed in [80, 81]. In addition, our results are also in accordance with the measurements of other observables at $N_\mathrm{c} = 3$, which conclude that finite volume effects are invisible as soon as $\beta/N < 1$ [82]. To obtain an infinite-volume estimate, we fit a constant to the data in the range

$$\frac{\beta}{NN_\mathrm{c}^2} < 0.1 \tag{4.35}$$

An other problem occurs when we conduct the extrapolation to the continuum, which we reach by fitting a second order polynomial to the divergence-subtracted data

$$d_1 + \frac{d_2}{\beta} + \frac{d_3}{\beta^2}. \tag{4.36}$$

To reliably obtain continuum values, we would like to perform the simulations with as large β as possible. Its maximum value is limited by the equation (4.35); as β grows the lattice volume grows as $\sim \beta^3$. Hence, the memory requirements of the simulation program soon outreach the capacity of computers. The minimum value is on the other hand limited by convergence of the series (4.36). Namely, there is a bulk phase transition, which is unique to the lattice theory and separates the weak and strong coupling regions. In Fig. 4.2, we have plotted the $P_G(N_\mathrm{c})$ as a function of $1/\beta$. The bulk phase transition is located slightly above $\beta \approx N_\mathrm{c}^2$. To be within the domain of convergence of the small beta expansion we require $\beta > N_\mathrm{c}^2$.

Summarising the requirements, we perform the simulations with β in the interval

$$N_\mathrm{c}^2 < \beta \lesssim \frac{N}{(N_\mathrm{c}/3)^2}. \tag{4.37}$$

[2] Almost similar algorithm was independently discovered by Kiskis, Narayanan and Neuberger [78]

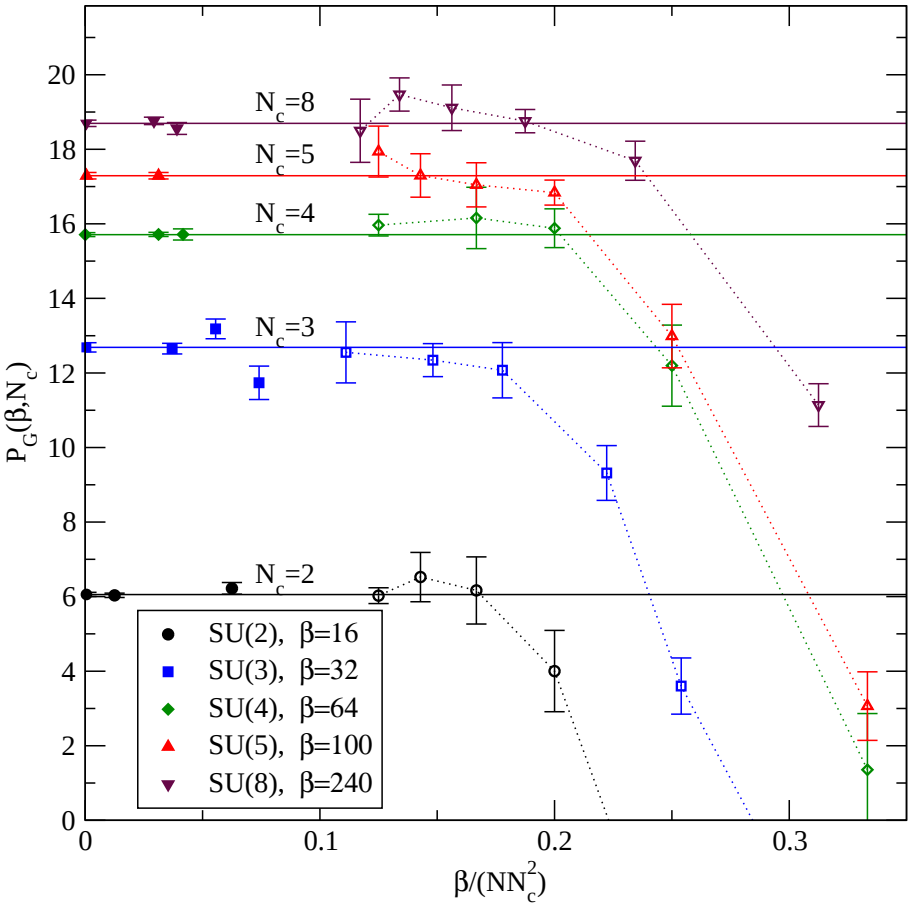

Figure 4.1: $P_G(\beta, N_c)$ as a function of $\beta/(NN_c^2)$ with different N_c and a constant β. Points denoted by open symbols correspond to low statistics simulations, performed to illustrate the exponential suppression of finite-volume effects. They are omitted in the extrapolation denoted by the solid horizontal line. The dotted line is for illustration purposes only. Finite-volume effects become visible around $\beta/(NN_c^2)$. The points on the vertical axis indicate the infinite-volume estimate, obtained by fitting a constant to the data in the range $\beta/(NN_c^2) < 0.1$.

4.3.3 Accuracy requirements

Because of the superrenormalizability of the theory additional loop corrections in MQCD are always one order higher in lattice spacing a than at the original order. This allows us to rigorously convert the measurements from lattice regularisation scheme to $\overline{\text{MS}}$ (or to some other continuum scheme). However, the conversion becomes challenging, if we consider a quantity with a high degree of divergence like the conversion between the plaquette expectation value and $B_G(N_c)$. We have to subtract many orders of divergent terms in order to obtain the conversion to the continuum regularization scheme. Obviously, we want to perform the simulations with as small lattice spacing a (large β) as possible to obtain a solid continuum limit. Therefore the subtraction of equation (4.20) leads to a major significance loss. For example, in the case of SU(4) the largest β used was $\beta = 100$, in which case the leading subtracted term in equation (4.20) $\sim c_1/\beta$ was six orders of magnitude larger than the signal we were interested in, which

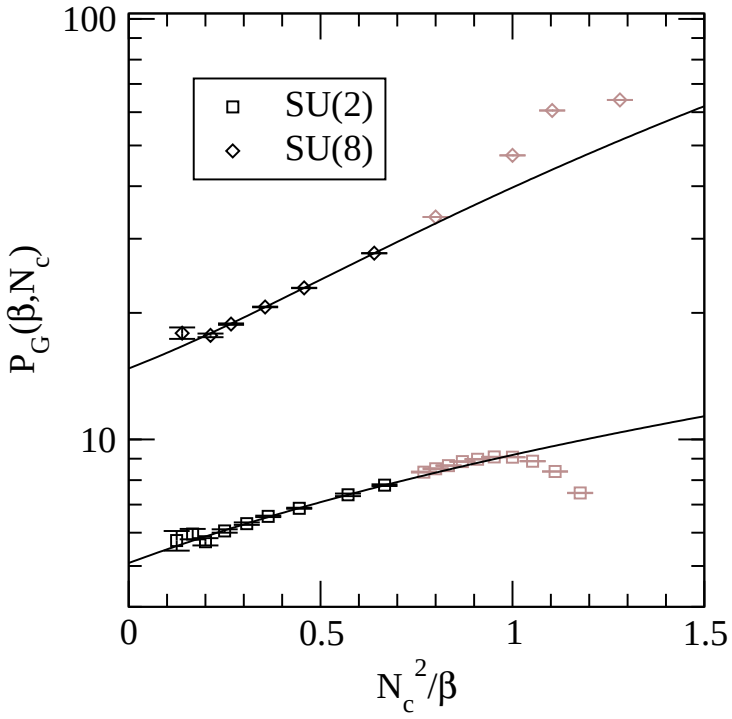

Figure 4.2: The bulk phase transition is located around $\beta \approx N_c^2$. Simulations denoted with the lighter color are left out of the continuum extrapolation.

was $\sim 1/\beta^4$. Therefore, to obtain a physically meaningful input, the relative error on our measurements should be smaller than one part in ten million. In addition, we also have to know the coefficients c_i with a good precision, see Fig. 4.3.

4.3.4 The result

After continuum extrapolation we studied the N_c dependence of our observable. As expected, the leading order contribution to P_G is a constant (see chapter 4.2.1). Our resolution is good enough to fit the next-to-leading order term. A polynomial in $1/N_c^2$ represents the data well, see Fig. 4.4 and [2]. As final result, we obtain

$$B_G(N_c) + \left(\frac{43}{12} - \frac{157}{768}\pi^2\right) c_4' = P_G(\infty, N_c) = 15.9(2) - 44(2)/N_c^2. \tag{4.38}$$

At the physical $N_c = 3$ we get

$$B_G(3) + \left(\frac{43}{12} - \frac{157}{768}\pi^2\right) c_4' = 11.0 \pm 0.3, \tag{4.39}$$

which is consistent with the calculation, where the values are evaluated in $N_c = 3$ simulations only. The value obtained in Ref. [1] is

$$B_G(3) + \left(\frac{43}{12} - \frac{157}{768}\pi^2\right) c_4' = 10.7 \pm 0.4. \tag{4.40}$$

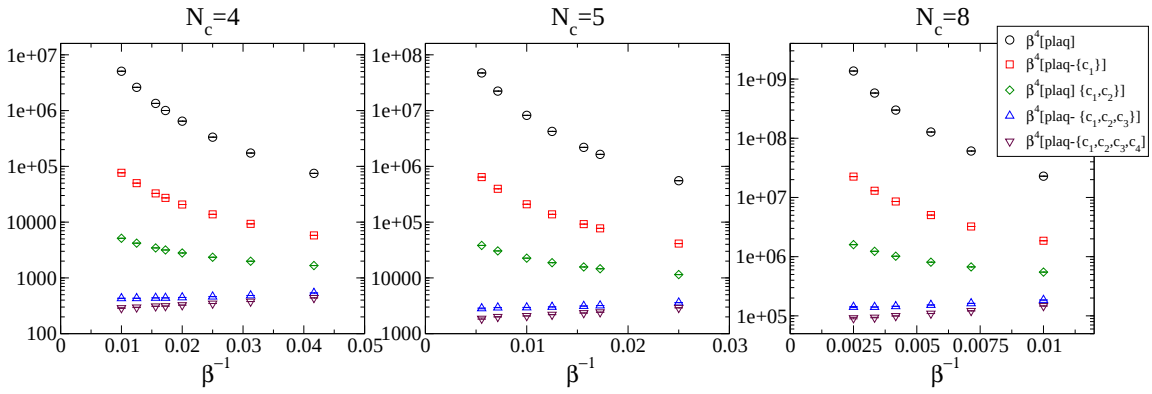

Figure 4.3: Significance loss due to the subtraction of lattice artifacts displayed in equation (4.20). The physical signal is many orders of magnitude smaller than number actually measured.

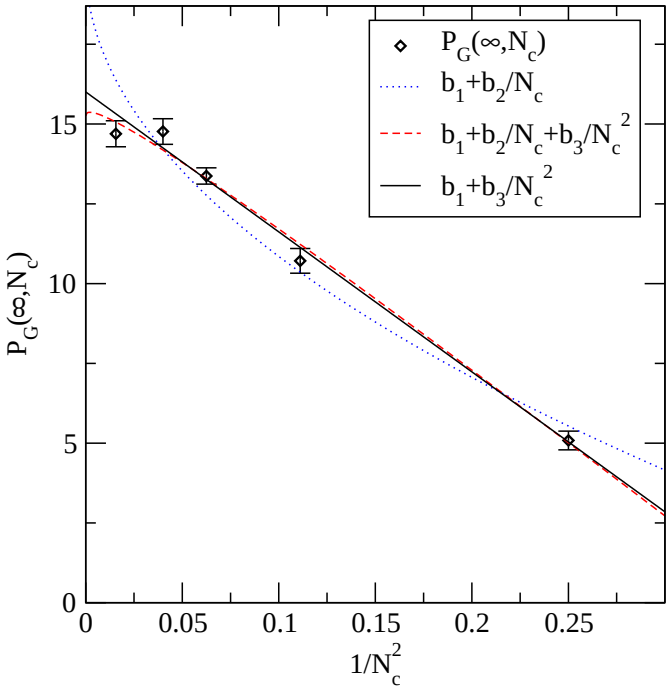

Figure 4.4: Comparison of different fitting functions for the next to leading order corrections of $P_G(\infty, N_c)$. Our data favors a zero $1/N_c$-term.

4.4 Consistency of the result

We have calculated the non-perturbative input to the QCD-pressure. Then, by calculating the unknown matching coefficients, we obtain the pressure up to the order g^6, which hopefully is close to the 4d-lattice results at low temperatures. However, it is important to perform some consistency checks to validate our results, especially because the convergence of the series is bad as one can see, e.g., from the left panel of Fig. 3.1. The order-by-order behaviour of the pressure is not systematic, and the low-temperature behaviour changes qualitatively at order $\mathcal{O}\left(g^3\right)$ and $\mathcal{O}\left(g^5\right)$.

Hence, we should estimate the size of the higher order contributions. The bad convergence of the series is associated with the bad convergence of the EQCD contribution, p_{M}. Indeed, the orders which change the low temperature behaviour, g^3 and g^5 are from EQCD, whereas the moderately changing orders obtain contributions from both hard and soft modes. Hence, studying the convergence of the series in EQCD provides a good approximation for the convergence of the whole series. We also note that the EQCD correction to the result starts from order g^7 whereas the first hard mode correction is order g^8.

In EQCD we can perform simulations at arbitrary high temperature or small coupling, and thus we can compare the results rigorously with perturbation theory and obtain an estimate of the size of the higher order contributions [49]. The procedure is as follows. Let us define a dimensionless EQCD free energy using the ratios of equation (3.19) at zero chemical potential.

$$\mathcal{F}(x,y) = \frac{f^{\mathrm{pert}}}{g_3^6} + \Delta\mathcal{F}(x,y), \tag{4.41}$$

where $f^{\mathrm{pert}} = -p_M/T$ and $\Delta\mathcal{F}(x,y)$ is the difference between the perturbation theory and the correct answer. To approximate the size of $\Delta\mathcal{F}(x,y)$, we perform lattice simulations. The free energy $\mathcal{F}(x,y)$ can not be directly measured from the lattice because it can not be normalized, but we can measure its derivatives. Hence, we write

$$\Delta\mathcal{F}_{\overline{\mathrm{MS}}}(x,y) = \Delta\mathcal{F}_{\overline{\mathrm{MS}}}(x_0,y_0) + \int_{y_0}^{y} \mathrm{d}y \left(\frac{\Delta\partial\mathcal{F}_{\overline{\mathrm{MS}}}(x,y)}{\partial y} + \frac{\mathrm{d}x}{\mathrm{d}y}\frac{\partial\mathcal{F}_{\overline{\mathrm{MS}}}(x,y)}{\partial x} \right) \tag{4.42}$$

The partial derivatives appearing here are the condensates

$$\frac{\Delta\partial\mathcal{F}_{\overline{\mathrm{MS}}}(x,y)}{\partial y} = \left\langle \frac{\mathrm{Tr}[A_0^2]}{g_{\mathrm{E}}^2} \right\rangle_{\overline{\mathrm{MS}},\,\mathrm{latt}} - \left\langle \frac{\mathrm{Tr}[A_0^2]}{g_{\mathrm{E}}^2} \right\rangle_{\overline{\mathrm{MS}},\,\mathrm{pert}}, \tag{4.43}$$

and

$$\frac{\Delta\partial\mathcal{F}_{\overline{\mathrm{MS}}}(x,y)}{\partial x} = \left\langle \frac{(\mathrm{Tr}[A_0^2])^2}{g_{\mathrm{E}}^4} \right\rangle_{\overline{\mathrm{MS}},\,\mathrm{latt}} - \left\langle \frac{(\mathrm{Tr}[A_0^2])^2}{g_{\mathrm{E}}^4} \right\rangle_{\overline{\mathrm{MS}},\,\mathrm{pert}}, \tag{4.44}$$

which can be measured on the lattice, and again because of the superrenormalizability of EQCD, we can convert them to $\overline{\mathrm{MS}}$ by calculating the difference of the renormalization schemes in the limit $a \to 0$. The integration constant $\Delta\mathcal{F}_{\overline{\mathrm{MS}}}(x_0,y_0)$ is the non-perturbative contribution obtained from MQCD simulations.

The project described above is not yet fully completed due to the large accuracy requirements needed to obtain a reliable and well behaving difference between the lattice simulations and perturbation theory in EQCD. However, in the next chapter we will calculate the quark number susceptibility, which also provides a reliability check for perturbation theory and dimensional reduction.

Chapter 5

The diagonal and off-diagonal quark number susceptibilities

The quark (baryon) number susceptibility is directly related to the event-by-event fluctuations observed in heavy ion collision experiments [20] and can provide a signature for the formation of QGP. Thus, it is of significant interest to calculate it theoretically as accurately as possible. Hence, several calculations of susceptibility using lattice simulations [83, 84, 85, 86, 87, 88] and perturbation theory have been published [54, 89].

In this chapter, we will discuss the calculation of the diagonal and off-diagonal quark number susceptibilities in the framework of EQCD. First we will derive an expression for the susceptibility in EQCD. The finite chemical potential results are obtained by performing simulations using imaginary chemical potential and then analytically continuing the results to real chemical potentials. In the end, we compare our results with other 4d lattice simulations.

5.1 Susceptibilities in EQCD

We are going to study the susceptibilities in the case of $N_\mathrm{c} = 3$ and $N_\mathrm{f} = 2$. The $\bar{\mu}$ dependence of the dimensionless couplings of Eq. (3.19) can be written as

$$\begin{aligned} g_\mathrm{E}^2 &= g_\mathrm{E}^2|_{\mu=0} \left(1 - \sum_{i=1}^{2} \frac{\mathcal{D}(\bar{\mu}_i)}{7} x\right) \\ x &= x|_{\mu=0} \left(1 - \sum_{i=1}^{2} \frac{\mathcal{D}(\bar{\mu}_i)}{7} x\right) \\ y &= y|_{\mu=0} \left(1 + \sum_{i=1}^{2} \frac{3}{8}\bar{\mu}^2\right) \equiv y_0 \left(1 + \sum_{i=1}^{2} \frac{3}{8}\bar{\mu}^2\right) \\ z &= \sum_{i=1}^{2} \frac{\bar{\mu}_i}{3\pi} \left(1 + \frac{27}{14} x\right). \end{aligned} \tag{5.1}$$

The corrections are of relative order $\mathcal{O}\left(x^2\right)$. For simplicity, we will ignore also the terms of $\mathcal{O}\left(x\right)$ in g_E^2, x , and z. Naturally, this effects our results somewhat. At the smallest temperatures we consider $x \sim 0.1$. The relative changes in z are larger than those in x and g_E^2, because $2/7\mathcal{D}(\bar{\mu})x < 1$ for all the values of $\bar{\mu}$ we consider. The relative change in z can be even around

20%. However, we expect the effect of the approximation to be smaller than our statistical errors, since the entire result is dominated by the value of y as will be shown later.

Following the equation (2.6), the susceptibility is the second derivative of pressure with respect to the quark chemical potential

$$\chi_{\mathrm{E,ij}} = \frac{1}{V}\frac{\partial^2}{\partial\bar{\mu}_i\partial\bar{\mu}_j}\ln\mathcal{Z} = \frac{1}{V}\frac{\partial^2}{\partial\bar{\mu}_i\partial\bar{\mu}_j}\ln\int\mathcal{D}A_k\mathcal{D}A_0\exp\left(-S_{\mathrm{E}}\right), \tag{5.2}$$

where i, j stands for quark flavors u and d. Thus, there are two independent components of the susceptibility: diagonal ($i = j$) and off-diagonal ($i \neq j$).

Using the shorthand notation for the (dimensionless) volume averages

$$\hat{A}_0^n \equiv \frac{1}{g_3^n V}\int d^3x\ \mathrm{Tr}A_0^n(x), \tag{5.3}$$

and defining the condensates

$$\begin{aligned}
K_1 &= \langle\hat{A}_0^2\rangle \\
K_2 &= Vg_3^6\left(\langle(\hat{A}_0^3)^2\rangle - \langle\hat{A}_0^3\rangle^2\right) \\
K_3 &= Vg_3^6\left(\langle(\hat{A}_0^2)^2\rangle - \langle\hat{A}_0^2\rangle^2\right) \\
K_4 &= Vg_3^6\left(\langle\hat{A}_0^3\hat{A}_0^2\rangle - \langle\hat{A}_0^3\rangle\langle\hat{A}_0^2\rangle\right),
\end{aligned} \tag{5.4}$$

we can write the susceptibilities as

$$\frac{\chi_{\mathrm{E,ij}}}{g_3^6} = -\frac{3}{4}\delta_{ij}\ y_0\,K_1 - \frac{1}{9\pi^2}K_2 + \frac{9}{16}\bar{\mu}_i\bar{\mu}_j\,y_0^2\,K_3 + i\frac{1}{4\pi}(\bar{\mu}_i+\bar{\mu}_j)\,y_0\,K_4. \tag{5.5}$$

The peculiarity here is that the expectation value of K_4 is imaginary even if the condensates themselves are purely real.

5.2 The finite density simulations

At non-zero μ, EQCD suffers from sign problem as well. Because of the imaginary term in the EQCD action at non-zero μ, the measure is not positively definite, and standard Monte Carlo techniques fail. There are some ideas, how to circumvent this problem. We will introduce the most popular ones from the viewpoint of EQCD. For a good review on the subject in QCD, see [90].

5.2.1 Reweighting

Reweighting is based on the following idea. If we have measured an expectation value $\langle O\rangle_{\lambda_0}$ with coupling λ_0, we obtain the expectation value with another coupling λ using the following identity

$$\langle O\rangle_\lambda = \frac{\langle Oe^{\Delta S}\rangle_{\lambda_0}}{\langle e^{\Delta S}\rangle_{\lambda_0}}, \tag{5.6}$$

where ΔS is the difference between the action with coupling λ and λ_0. One can also reweight with respect to multiple couplings at the same time.

In order for the reweighting to provide reliable results, fluctuations in simulations with coupling λ_0 must overlap with those performed λ. The difference behaves approximately as

$$\Delta\lambda \sim \frac{1}{\sqrt{V}} \tag{5.7}$$

when the system is away from a phase transition, and as

$$\Delta\lambda \sim \frac{1}{L^\kappa} \tag{5.8}$$

when the system is at a critical point. Here κ is some critical exponent.

To study non-zero μ, one performs simulations with $\mu = 0$ and then reweights them to the desired value. In EQCD, we have an additional difficulty since we have to stay on the "constant physics curve" (3.22). Therefore, we have to reweight with respect to two couplings z and y. The reweighting with respect to y is problematic, because the expectation values are sensitive to it, and hence it is possible to reweight only to small values of μ. Remember that we need rather large volumes $V = 256^3$ to obtain a reliable continuum limit and the fluctuations die out as $\sim 1/\sqrt{V}$. Naturally, we could perform simulations using the physical value y calculated with the value of μ, to which we are going to reweight. In this case we would have to perform a unique simulation for each (T,μ)-pair. This does not render the method useless, but on the other hand there are more effective methods as well that can be utilized here as will be explained later.

If one is interested in quantities requiring less accuracy than our observable, then reweighting with respect to both x and y becomes a feasible option. This was the case in [50], where the measured quantities were screening lengths and the largest simulation volume used was $V = 40^3$, whereas we need volumes up to $V = 256^3$. Their conclusion was that reweighting is possible for chemical potentials up to $\mu/T = 2.0$. A naive estimate in our case would allow us to reweight only to chemical potentials $\mu/T \approx 0.1$.

5.2.2 Taylor expansion

The Taylor expansion method is very similar to the one we are going to utilize, and is based on the same fact: On the lattice, the partition function $Z(x, y(\bar{\mu}), z(\bar{\mu}))$ is an analytic function of its parameters. Hence, we can expand the susceptibility around $\mu = 0$

$$\chi_3(z) = a_0 + a_2\bar{\mu}^2 + a_4\bar{\mu}^4 + \dots. \tag{5.9}$$

The coefficients a_i are increasingly more complex functions of the A_0-condensates. Because $\langle \mathrm{Tr} A_0^n \rangle$ vanishes for odd n at $\mu = 0$, the odd terms vanish. Again, one could improve the accuracy by performing simulations by fixing y first and expanding only in z . This would also simplify the Taylor coefficients considerably, because they would be only $2n$-moments of $\langle \mathrm{Tr}_0^3 \rangle$.

5.2.3 Analytic continuation

In standard analytic continuation the observable is again Taylor expanded about $\mu = 0$, but this time the coefficients are calculated from the simulations with imaginary chemical potential

$$\chi_3(z) = b_0 + b_2\bar{\mu}^2 + b_4\bar{\mu}^4 + \dots = b_0 - b_2(i\bar{\mu})^2 + b_4(i\bar{\mu})^4. \tag{5.10}$$

The calculation with imaginary chemical potential provides a better control of the curvature of the observable as $\bar{\mu}$ grows.

However, as mentioned above, the results are dominated by the $K_1 \sim \langle \mathrm{Tr} A_0^2 \rangle$-term. In pure analytic continuation, we should simulate with

$$y \to y \left(1 + \sum_{i=1}^{2} \frac{3}{8} (i\bar{\mu})^2 \right), \tag{5.11}$$

but we fix y to its physical value and perform the analytic continuation only about z. If we then expand each condensate K_i separately, we note that the z dependence of the condensates is very weak and we have to expand only to a very low order

$$K_1 = a_1 + a_2 z^2 \qquad K_3 = a_4 \tag{5.12}$$

$$K_2 = a_3 \qquad K_4 = \frac{\partial C_1}{\partial (iz)} = -2ia_2 z. \tag{5.13}$$

Note that because K_4 is $\sim \langle \mathrm{Tr} A^5 \rangle$, it is a series in odd powers of z. We assume that K_2 and K_3 are independent of z, which is true within the statistical accuracy we can reach as we will demonstrate later by performing simulations with constant x and y and varying z only. The z dependence of K_1 is also rather small, and only visible at smallest temperatures, but we will anyhow include it.

Finally, we can write the analytically continued final result as

$$\begin{aligned} \frac{\chi_{3,ij}(z)}{g_3^6} = &- \frac{3}{4} \delta_{ij} \; y_0 \left(K_1 + z K_4 \right) - \frac{1}{9\pi^2} K_2 \\ &+ \frac{9}{16} \bar{\mu}_i \bar{\mu}_j \, y_0^2 \, K_3 + \frac{1}{4\pi} (\bar{\mu}_i + \bar{\mu}_j) \, y_0 K_4 \,, \end{aligned} \tag{5.14}$$

where the condensates K_i have been measured at imaginary chemical potential iz

5.2.4 Imaginary μ and the phase diagram of EQCD

As described in chapter 3.3, to describe 3d-physics correctly, EQCD must stay in its symmetric phase $\langle \mathrm{Tr} A_0^3 \rangle = 0$. The finite chemical potential alters the picture somewhat. First, the order parameter $\langle \mathrm{Tr} A_0^3 \rangle$ obtains a non-zero expectation value, which is however rather small and therefore does not cause any problems.

A more significant change to the phase diagram is caused by the change of the mass parameter y, as μ is altered. In the case of standard analytic continuation, y would be smaller bringing the "constant physics curve" deeper into the broken phase. The phase transition point was calculated to be $\bar{\mu} = 1/3$ in [51]. However, for our method of analytic continuation this problem is completely avoided: Because we calculate $y(\mu)$ with real μ, the value of y increases as μ increases. Thus, the physical symmetric phase remains stable at all values of μ.

5.3 Matching to QCD

The results of the EQCD simulations must be matched back to QCD. Being perturbative in nature the procedure produces some error to the result. The susceptibility in QCD can be written in terms of the EQCD susceptibility and the matching terms as follows

$$\frac{\chi_{ij}}{T^2} = \frac{g_3^6}{\pi^2 T^3} \chi_{3,ij} + \frac{\partial^2}{\partial \mu_i \partial \mu_j} \Delta p, \tag{5.15}$$

where

$$\Delta p = p_{\rm E} - \frac{g^4}{(4\pi)^4} d_{\rm A} C_{\rm A} \alpha_{\rm E5} + \mathcal{O}\left(g^6\right) \tag{5.16}$$

is the perturbative 3d↔4d matching coefficient for the pressure.

However, there is an additional complication in the matching of the lattice results. In perturbation theory, one obtains an expression like, e.g., $Cg_{\rm E}^6$, which can be converted to full QCD by substituting to it the equation (3.12), whereas on the lattice side one obtains a number $L(x, y, z)$. To match this number to QCD, we need to know the actual value of the QCD coupling g that the parameters correspond to. The coupling can be resolved by first using equation (3.21) to obtain T, from which g can be calculated. Then we can utilize equation (5.15) to obtain the physical result. However, because the relations have been calculated in perturbation theory, all of these steps are approximative. Therefore, Δp and our measurements are calculated at slightly different couplings g. The effect of this difference grows as $T \to T_{\rm c}$, and to minimise it, we perform the matching for the non-perturbative parts only

$$\frac{\chi}{T^2} = \frac{g_3^6}{\pi^2 T^3} \left(\chi_3^{\rm latt} - \chi_3^{\rm pert})\right) + \frac{\chi^{\rm pert}}{T^2}. \tag{5.17}$$

Here, $\chi_3^{\rm pert}$ and $\chi^{\rm pert}$ are 3d and 4d perturbative results.

There are two additional source of errors in the matching procedure. The first one is that the the perturbative series, and hence the matching, is known only up to order $g^6 \ln 1/g$. Comparison with 4d-lattice data [85, 86] indicates that the size of higher order terms is comparably small. The second one is that to match the result with physical temperature, we need to know $\Lambda_{\overline{\rm MS}}$. We use the value $\Lambda_{\overline{\rm MS}} = 245\,{\rm MeV}$, which has been obtained from lattice simulations with 2 light Wilson quarks [91]. To compare with 4d-lattice results, which have usually been normalized to the critical temperature, we choose $T_{\rm c} = 170$ MeV, yielding the ratio $T_{\rm c}/\Lambda_{\overline{\rm MS}} = 0.7$. This is compatible with the results of [92], $r_0 T_c = 0.438$ combined with [91] $r_0 \Lambda_{\overline{\rm MS}} = 0.62$, where r_0 is hardronic radius. Our results are in fact more sensitive to the selection of the scale $\Lambda_{\overline{\rm MS}}$ than the size of the order g^6 contribution, if the coefficient of the g^6-term is taken to be of the same order as coefficients of the lower order contributions.

5.4 Lattice $\overline{\rm MS}$ relations for condensates K_i

In analogy with the MQCD case, the lattice $\overline{\rm MS}$ relations of the observables can be derived by considering the difference of the free energy in the two schemes. The difference can be parametrised as

$$\begin{aligned}
\Delta f \equiv & f_a(m_{\rm E}^2, g_{\rm E}^2, \lambda_{\rm E}) - f_{\overline{\rm MS}}(m_{\rm E}^2, g_{\rm E}^2, \lambda_{\rm E}) && (5.18)\\
= & \frac{d_{\rm A}}{4\pi}\left[C_{1,0}\frac{1}{a^3} + D_{1,0}\frac{m_{\rm E}^2}{a}\right] && (5.19)\\
& + \frac{d_{\rm A}}{(4\pi)^2}\left[C_{2,0}\frac{g_{\rm E}^2}{a^2} + C_{2,1}\frac{\lambda_{\rm E}}{a^2} + D_{2,0} g_{\rm E}^2 m_3^2 + \lambda_{\rm E} m_{\rm E}^2\right] && (5.20)\\
& + \frac{d_{\rm A}}{(4\pi)^3}\left[C_{3,0}\frac{g_{\rm E}^4}{a} + C_{3,1}\frac{g_{\rm E}^2\lambda_{\rm E}}{a} + C_{3,2}\frac{\lambda_{\rm E}^2}{a}\right] && (5.21)\\
& + \frac{d_{\rm A}}{(4\pi)^4}\left[C_{4,0} g_{\rm E}^6 + C_{4,1} g_{\rm E}^4 \lambda_{\rm E} + C_{4,2} g_{\rm E}^2 \lambda_{\rm E}^2 + C_{4,3}\lambda_{\rm E}^3 + E_{2,0}\gamma_{\rm E}^2\right], && (5.22)
\end{aligned}$$

where $C_{i,0}$ are the same coefficients as those denoted by C_i in the case of MQCD.

The continuum relations for the condensates can be derived by differentiating Δf with respect to the couplings. Using dimensionless variables we have

$$\Delta K_1 = \frac{\partial \Delta \mathcal{F}}{\partial y} \qquad \Delta K_3 = \frac{\partial^2 \Delta \mathcal{F}}{\partial y^2} \tag{5.23}$$

$$\Delta K_2 = -\frac{\partial^2 \Delta \mathcal{F}}{\partial z^2} \qquad \Delta K_4 = i\frac{\partial^2 \Delta \mathcal{F}}{\partial y \partial z} \tag{5.24}$$

In the limit the lattice spacing $a \to 0$ (or $\beta \equiv 6/(g_{\mathrm{E}}^2 a) \to \infty$) we obtain following relations [42, 61, 93]

$$\begin{aligned} K_{1,\overline{\mathrm{MS}}} &= K_{1,a} - \tilde{c}_1\beta - \tilde{c}_2\left(\ln\beta + \tilde{c_2}'\right) + \mathcal{O}(1/\beta), \\ K_{2,\overline{\mathrm{MS}}} &= K_{2,a} - \left[\bar{c}_2\left(\ln\beta + \bar{c}_2'\right)\right] + \mathcal{O}(1/\beta), \end{aligned} \tag{5.25}$$

$$\begin{aligned} K_{3,\overline{\mathrm{MS}}} &= K_{3,a} + \mathcal{O}(1/\beta), \\ K_{4,\overline{\mathrm{MS}}} &= K_{4,a} + \mathcal{O}(1/\beta), \end{aligned} \tag{5.26}$$

where the values of the coefficients are given in Appendix A.

As can be seen from equations (5.25), the significance loss due to the subtraction of lattice divergences is much milder in K_i's than in the case of $B_G(N_{\mathrm{c}})$. However, because we want to compare lattice results with the perturbation theory result of EQCD the accuracy requirements are still extremely high.

5.5 Simulation algorithms

To simulate EQCD we need efficient update algorithms for the adjoint A_0 field. Because A_0 couples to the gauge field, the HB and OR gauge field update algorithms must be adjusted. However, the changes are minor. We calculate the update using standard techniques described in chapter 4.3 and then perform an accept/reject check including the coupling to adjoint A_0 field.

The adjoint A_0 fields themselves can be updated using pseudo-HB and -OR algorithms[1]. The local action can be written in the form[2]

$$S_{\mathrm{A,local}}(\mathbf{x}) = \beta_2 \mathrm{Tr}\left[A_0(\mathbf{x}) - \frac{\beta_{\mathrm{A}}}{2\beta_2} X_{\mathrm{adj}}(\mathbf{x})\right]^2 - \beta_3 \mathrm{Tr}[A_0^3(\mathbf{x})] + \beta_4 (\mathrm{Tr}[A_0^2(\mathbf{x})])^2, \tag{5.27}$$

where β_i are the couplings on the lattice trivially calculated from (4.13) and X_{adj} is the staple for A_0

$$X_{\mathrm{adj}}(\mathbf{x}) = \sum_{k=1}^{3}\left[U_k(\mathbf{x})A_0(\mathbf{x}+\hat{k})U_k^\dagger(\mathbf{x}) + U_k^\dagger(\mathbf{x}-\hat{k})A_0(\mathbf{x}-\hat{k})U_k(\mathbf{x}-\hat{k})\right]. \tag{5.28}$$

Then both the HB and OR algorithms are easy to implement for the quadratic part, and one can perform a metropolis-check with cubic and quartic terms. To be more precise, the HB algorithm works as follows. We generate a new field A_{new} with

$$A^a_{0,\mathrm{new}} = \frac{\beta_{\mathrm{A}}}{2\beta_2} X^a_{\mathrm{adj}} + \frac{1}{\sqrt{\beta_2}} R_{\mathrm{gauss}}, \tag{5.29}$$

[1] They are pseudo algorithms since at the end a Metropolis check is required.

[2] Here we have substituted $z = iz$

where R_{Gauss} is a gaussian random number between -1 and 1. The new field is updated with the probability

$$P_{\mathrm{acc}} = \exp\left[\beta_4(\mathrm{Tr}[A^2_{0,\mathrm{old}}]^2 - \mathrm{Tr}[A^2_{0,\mathrm{new}}]^2) - \beta_3((\mathrm{Tr}[A^3_{0,\mathrm{old}}] - (\mathrm{Tr}[A^3_{0,\mathrm{new}}])\right], \tag{5.30}$$

where $A^a_{0,\mathrm{old}}$ is the old adjoint field. The OR algorithm is as straightforward. The new matrix is generated as

$$A^a_{0,\mathrm{new}} = \frac{\beta_{\mathrm{A}}}{\beta_2} X^a_{\mathrm{adj}} - A^a_{0,\mathrm{old}}, \tag{5.31}$$

which does not change the magnitude of the quadratic part of the local action. The $A^a_{0,\mathrm{new}}$ is then accepted with the probability (5.30).

We performed one HB for four OR updates for both the gauge and the adjoint fields. Because the gauge fields have considerably smaller autocorrelation times, they were only updated in one direction each time. The acceptance of the Metropolis check (5.30) was good, being always over 95%, regardless of the parameter values. The autocorrelation times of the simulations grows when β increases and y decreases. The smallest autocorrelation times were around 1 ($\beta = 32$ $y = 6.62$) and the largest around 300 ($\beta = 120$ $y = 0.36$).

5.6 Results of lattice simulations

The details of the simulation parameters used and the continuum extrapolation are described in [3]. Instead of extrapolating the condensates separately, we calculate the susceptibility using equation (5.14) for each lattice spacing separately, after which we subtract lattice divergences, and perform the continuum extrapolation. This is more rigorous, because now the analytic continuation is performed for finite a, which guarantees analyticity of the expectation values.

The results are dominated by the condensate K_1. The condensate K_2 is rather small, but it is important for the off-diagonal susceptibility. At $\bar{\mu} = 0$, it provides the entire contribution for this quantity. The condensate K_3 (in addition to the change of y) describes the finite chemical potential dependence since it includes a factor $\bar{\mu}^2$. The condensate K_3 has relatively large errors, which hinders the precision of our result as $\bar{\mu}$ grows. The condensate K_4, which describes the effect of non-zero chemical potential as well, is negligible at all but the smallest temperatures, see Fig. 5.1 and Fig. 5.2.

5.6.1 Diagonal susceptibility

Our main results for the diagonal susceptibility are presented in Fig. 5.3 and Fig. 5.4. At zero $\bar{\mu}$, they agree with 4d-lattice at least as well as the 4d dynamical two flavor lattice results [83, 94] agree with each other. The deviation from perturbation theory is significant still at $T = 10T_{\mathrm{c}}$, indicating that the higher order perturbative contributions are important at experimentally accessible temperatures, see left panel of Fig. 5.3. Our results are somewhat sensitive to the used scale $T_c/\Lambda_{\overline{\mathrm{MS}}}$. The result of varying the scale about 15% is shown in the right panel of Fig. 5.3. The scale we use $T_c/\Lambda_{\overline{\mathrm{MS}}} = 0.7$ is close to optimal from the point of view of the agreement with 4d-simulations, and changes of about 10% do not effect the agreement considerably. One should also keep in mind that the order g^6 matching coefficient is still unknown, but our results indicate it to be rather small.

The finite μ effects are plotted in Fig. 5.4. In the left panel the results are normalized with respect to the Stefan-Boltzmann result

$$\chi_{\mathrm{SB}}(\mu) = T^2 + \frac{3}{\pi^2}\mu^2. \tag{5.32}$$

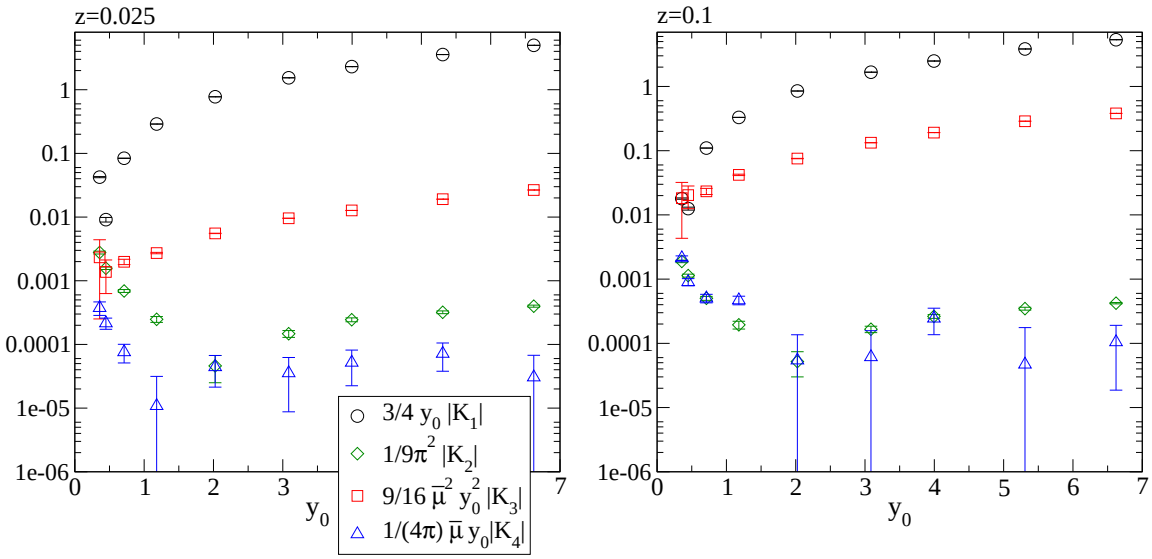

Figure 5.1: The magnitudes of the different terms contributing to the diagonal susceptibility. The change of the slope of $|K_1|$ at $y \approx 0.5$ and $|K_2|$ at $y \approx 2$ is due to a change of sign in the condensates themselves.

The deviation is large at low temperatures, but already at $T = 10T_c$ the Stefan-Boltzmann law describes the finite-μ behaviour well and around $T \sim 100T_c$ almost exactly. However, at low temperatures the μ dependence is in accordance with the lattice results of [85, 86], see the right panel of Fig. 5.4.

5.6.2 Off-diagonal susceptibility

The results for the off-diagonal susceptibility χ_{ud} are shown in Fig. 5.5 and Fig. 5.6. The EQCD results approach perturbation theory faster than in the case of the diagonal susceptibility being similar already at temperatures $\sim 10T_c$. At $\mu = 0$ and $T < 3T_c$, our results have a larger magnitude than those of 4d-lattice [85, 86] and perturbation theory, see the left panel of Fig. 5.6. There is a strong downward curvature as one approaches the critical temperature from above. The EQCD simulations seem to predict this behaviour, but at larger temperatures. Increasing $T_c/\Lambda_{\overline{\rm MS}}$ would bring results closer to each other, but for them to agree we need a rather large value $T_c/\Lambda_{\overline{\rm MS}} \approx 0.9$, and the higher temperature simulation results would still be somewhat below the 4d-lattice results. Naturally, this should be viewed as an indication that we are already at the border of the validity of dimensional reduction.

Nevertheless, the μ-dependence of $\chi_{\rm ud}$ is in accordance with the 4d lattice results [85, 86] already at $T \sim 1.32T_c$. The behaviour is plausible in the entire simulation range $0 \leq \mu_q/T \leq 2.22$; see the right panel of Fig. 5.6.

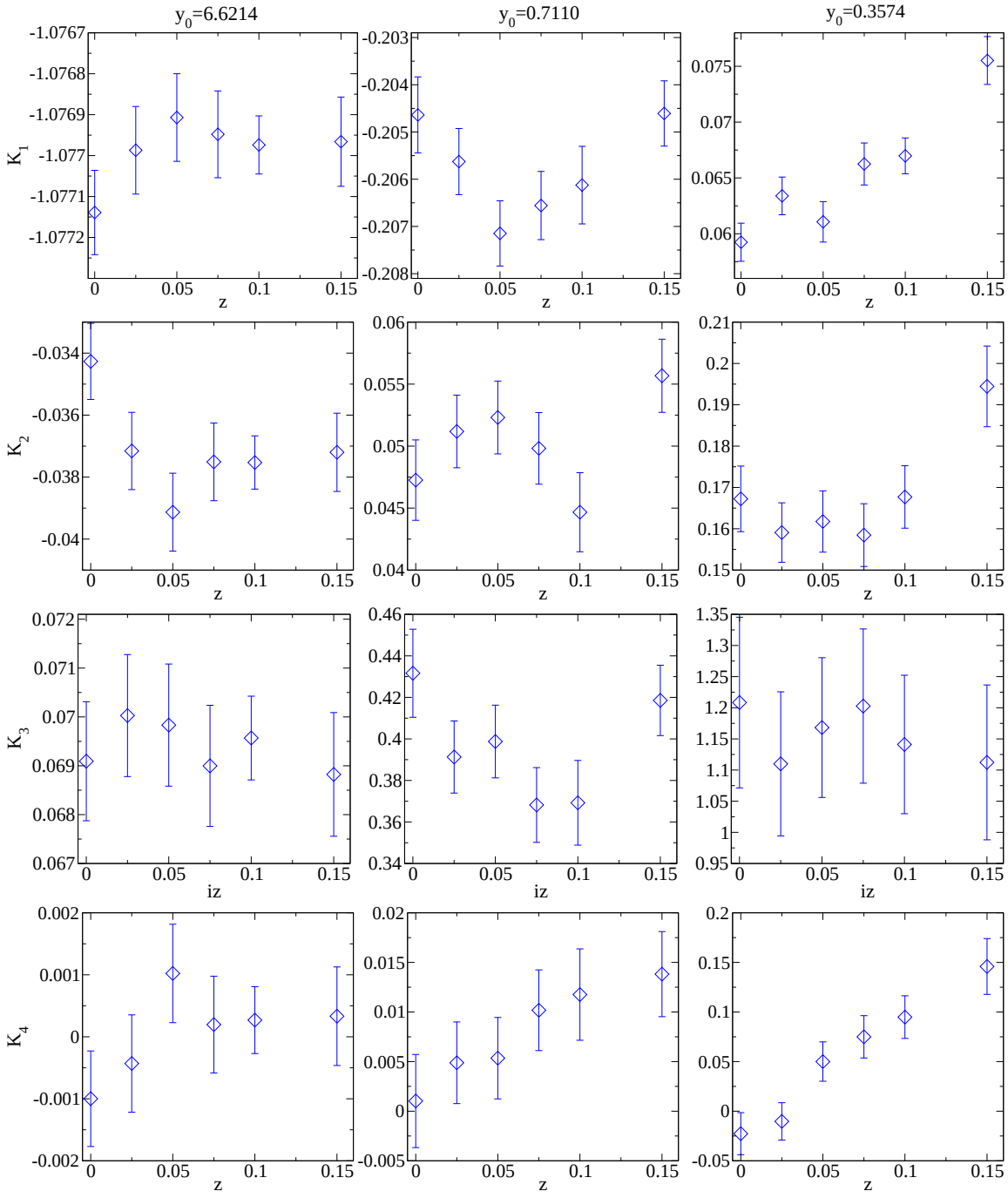

Figure 5.2: Simulations performed with three different pairs of (x, y) values while varying the chemical potential in the range $0 \leq z \leq 0.15$. The dependence of the chemical potential is only visible at smallest y (temperature), where it effects K_1 and K_4 only.

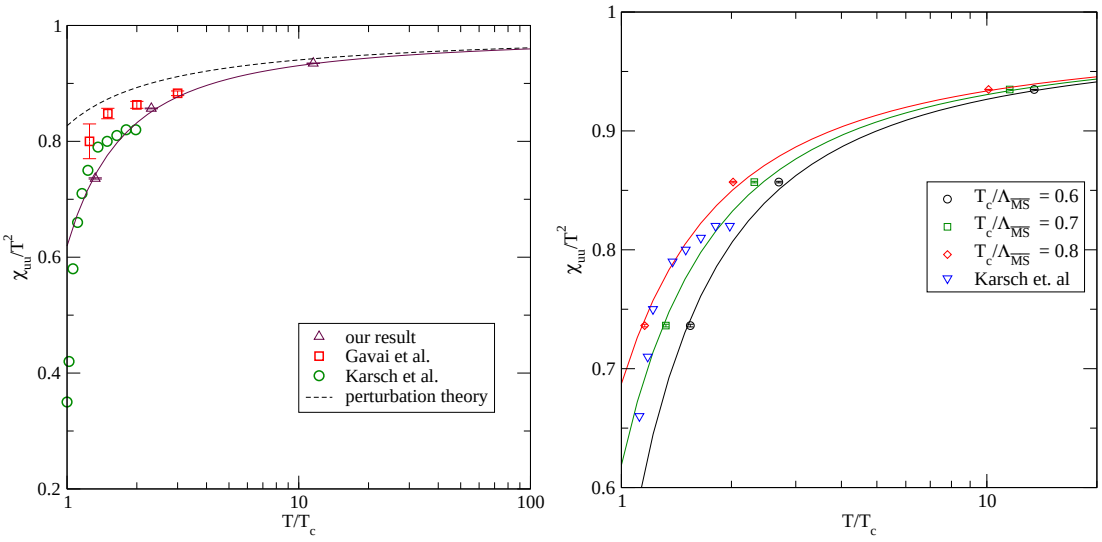

Figure 5.3: Left: The diagonal susceptibility at $\mu = 0$. The data points indicate the full EQCD result. The continuous line is a fit to our result, and the dashed line shows the perturbative result of [54]. The agreement with the 4d-lattice results of [83] and [94] is good. Right: Our result plotted with different values of the scale $T_c/\Lambda_{\overline{MS}}$. Again the solid lines show a fit to these result.

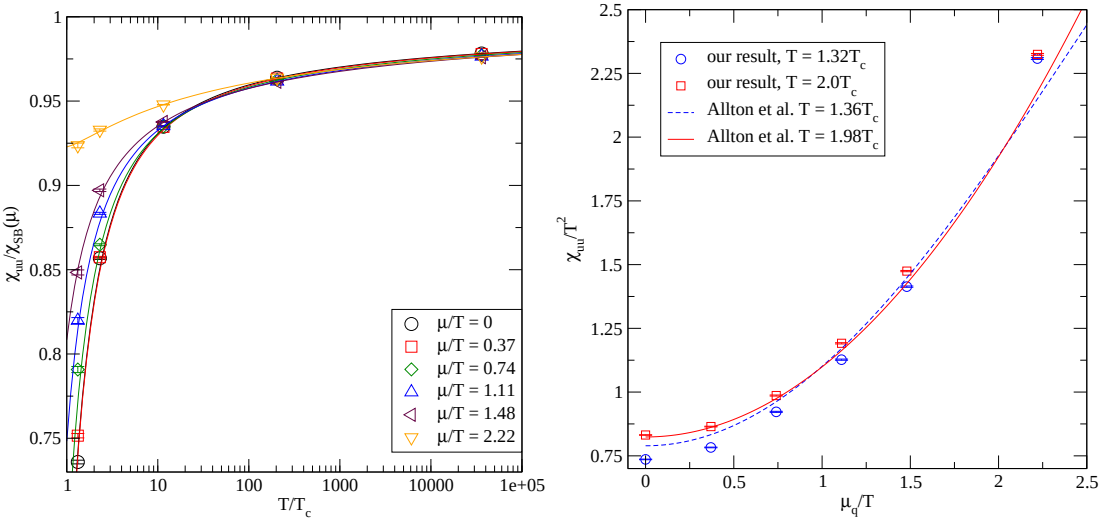

Figure 5.4: Left: The diagonal susceptibility at different values of μ, normalized to the Stefan-Boltzmann law. The deviation from Stefan-Boltzmann law is visible only at smallest temperatures. Right: The susceptibility at a constant temperature as a function of μ. The agreement with the 4d lattice results of [85, 86] is excellent.

.

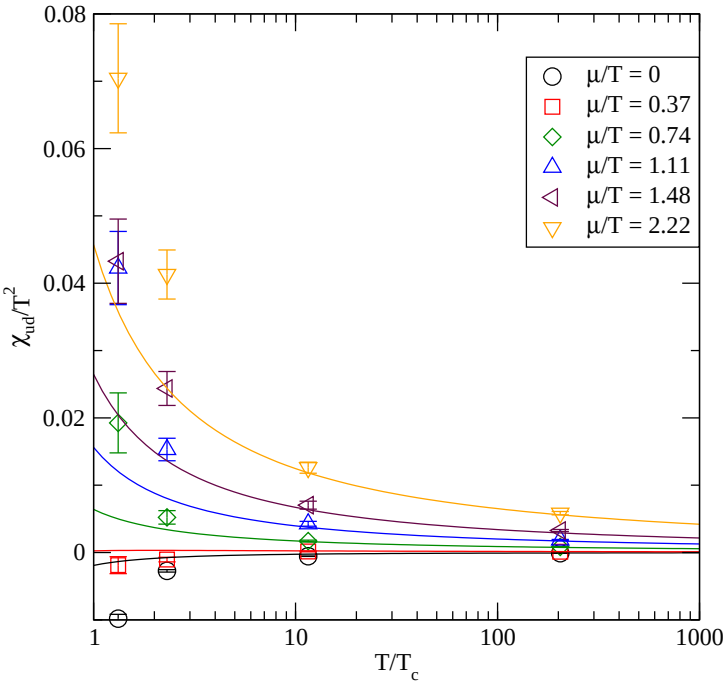

Figure 5.5: The off-diagonal susceptibility in 4d. At low temperatures the values differ significantly from perturbation theory, denoted by solid lines, but there is no deviation at $10T_c$ anymore.

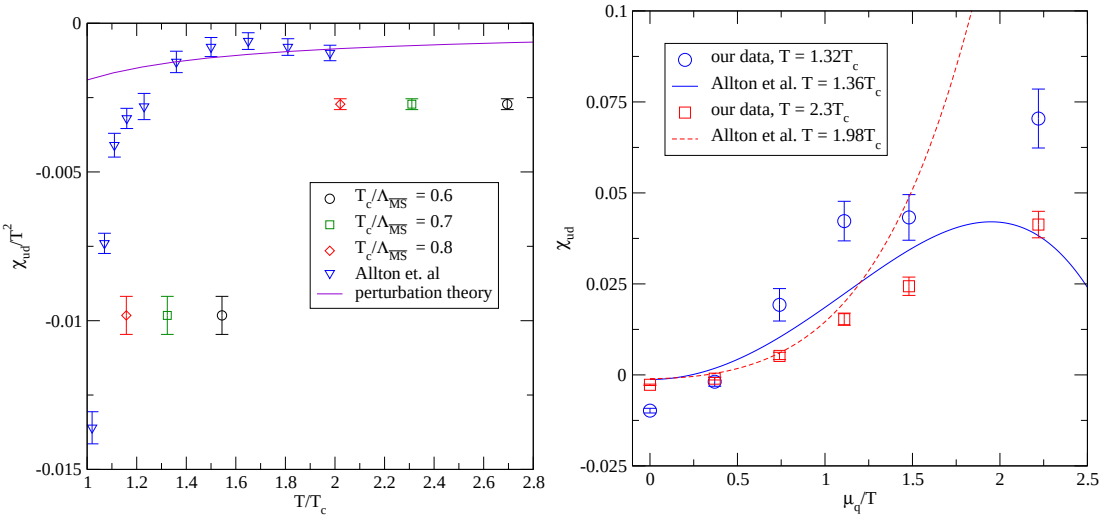

Figure 5.6: Left: The off-diagonal susceptibility in 4d at $\mu = 0$. The devitaion from lattice results of Allton et al.[85, 86] is large below $2T_c$. However, the curvature is correct. Right: Comparison of the finite μ behaviour of the EQCD results with those of Allton et al. [85, 86]

.

Chapter 6

Conclusions and Outlook

In this thesis, we have studied dimensionally reduced effective theories of high temperature QCD, EQCD and MQCD. MQCD was utilized to obtain the non-perturbative input to the QCD pressure by calculating the plaquette expectation value. This requires high precision numerical Monte Carlo simulations close to the continuum limit. The task is challenging because the conversion of the result to a continuum scheme requires a subtraction of perturbative terms up to 4-loop level, which leads to a major significance loss. After the lattice result is converted to $\overline{\mathrm{MS}}$, the full QCD pressure of order g^6 can be obtained by a further 4-loop computation of the unknown matching coefficient β_{E1}. The calculation of the missing matching coefficients seems a tedious task, but it is well-motivated since if the effect of the g^6 term is taken into account, perturbation theory might be applicable at surprisingly low, experimentally accessible, temperatures, as discussed in chapter 3.1, see also [32].

The accuracy of the perturbative expansion at 4-loop level can be quantitatively estimated through EQCD simulations. The bad convergence of perturbation theory can be traced back to the bad convergence of the series in EQCD. Because EQCD can be easily simulated in the entire parameter range where perturbation theory is valid, the difference of the lattice results and perturbation theory provides a good approximation for the sum of the higher order terms, starting at order g^7. However, this is the subject of still ongoing research work.

In this thesis, EQCD was utilized to calculate the quark number susceptibilities. Our results agree well with 4d lattice results of two light quark flavors. This demonstrates the wide range of applicability of the method. The diagonal susceptibility agrees with the 4d simulations by Allton et al. [85, 86] even below $2T_{\mathrm{c}}$. The results smoothly approach the perturbative results, but there is still a significant deviation at $10T_{\mathrm{c}}$. The off-diagonal susceptibility agrees with perturbation theory already at $10T_{\mathrm{c}}$. However, the agreement with [85, 86] is poor below $2T_{\mathrm{c}}$, which indicates that we are already at the border of the applicability of EQCD.

EQCD is also extremely well suited for the finite μ simulations. The main reason for this is that most of the finite μ effect is taken into account by changing the values of the coupling constant y, whereas the problematic imaginary term effects the results only marginally. We obtain a smooth behaviour in the whole parameter range of simulations and hence, we can conclude that EQCD is valid at at least to chemical potentials $\mu/T \sim 2.5$. This is in accordance with the results of [58] where it was concluded that EQCD is valid approach to arbitrary large values of μ/T as long as πT is the largest scale in the theory. More precisely $\pi T > m_{\mathrm{E}}$.

The significant difference between perturbation theory and the EQCD result for the susceptibility up to $10T_{\mathrm{c}}$ seems to argue against the possibility that the perturbative expansion of the pressure could be accurate already at order g^6. However, the order by order comparison

between the observables is misleading. The pressure obtains the first non-perturbative input at g^6, whereas the corresponding order for the susceptibility is g^8. According to the conjecture presented in [95], most of the dynamics of the dimensionally reduced theory has been accounted when all the scales have made their entrances in the result.

Our results support the conjecture to some extent. As can be seen from the Table 2 of [3], the terms of order g^8 are larger than those of order g^7. Naturally, this does not predict the magnitude of the higher order corrections since statistical errors in our data are too large to approximate them. Nevertheless, the fit up to order g^8 represents the data well and provides good agreement with 4d-lattice simulations down to temperatures $2T_\mathrm{c}$. The inclusion of even higher order terms in the fit does not alter the situation qualitatively. Hence, the perturbative result of the pressure up to order g^6 might well be a good approximation of the full result at experimentally accessible temperatures.

Appendix A

Lattice perturbation theory

To rigorously convert the lattice simulations to $\overline{\text{MS}}$ regularisation, we need to compute the observables in both lattice and $\overline{\text{MS}}$ regularisation. Then the conversion is provided by the difference of the results. Because of the superrenormalizability of EQCD and MQCD, there are divergent terms only up to a finite loop order. We will here review some of the calculations needed for the quantities in question [42, 96, 93, 97].

A.1 Plaquette expectation value

Let us first consider the case of MQCD, where we need to calculate the plaquette expectation value up to $\mathcal{O}\left(1/\beta^4\right)$. The leading order contribution $\sim 1/\beta$ can be obtained straightforwardly. Following [98], we parametrise the plaquette as

$$P = \exp(iT^a\omega_{\text{P}}^a), \tag{A.1}$$

where $\omega_{\text{P}}^a \in \mathcal{R}$. At leading order, the partition function becomes

$$Z = \int \mathcal{D}U \exp\left(-\frac{\beta}{4N_{\text{c}}}\omega_{\text{P}}^a\omega_{\text{P}}^a + \mathcal{O}\left(\beta\omega_{\text{P}}^4\right)\right). \tag{A.2}$$

The expression requires gauge fixing. However, in the leading order calculation we note that gauge fixing fixes one direction of the link matrices.

Expanding the link matrices near unity, the partition function can be written in quadratic form as

$$Z = C\int\prod_{ij}\mathrm{d}^{d_{\text{A}}}\omega_{ij}\exp\left[-\frac{1}{2}\beta\omega K^{-1}\omega + \mathcal{O}\left(\beta\omega^3\right)\right], \tag{A.3}$$

where K is the gauge boson propagator and the terms $\mathcal{O}\left(\beta\omega^3\right)$ generate the vertices. Because the integrand in equation (A.3) is Gaussian, the integration can be performed, resulting in

$$Z = C'\left|\frac{K}{\beta}\right|^{1/2}. \tag{A.4}$$

The matrix K has the dimensionality of the parameter space after gauge fixing. Hence, pulling β in front of the equation results

$$Z = C'|K|^{1/2}\beta^{d_{\text{A}}N^3}, \tag{A.5}$$

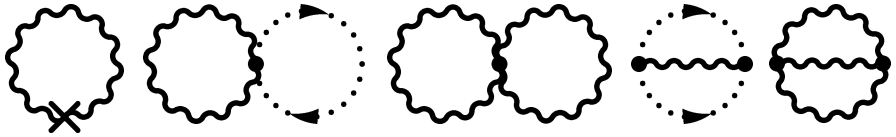

Figure A.1: Feynman diagrams needed to calculate c_2

where the result holds in three dimensions. Then, we obtain the average plaquette in the form

$$\begin{aligned} P &= -\frac{1}{3N^3}\frac{\partial}{\partial\beta}\ln Z \\ &= \frac{d_{\rm A}}{3}\frac{1}{\beta} + \mathcal{O}\left(\frac{1}{\beta^2}\right). \end{aligned} \tag{A.6}$$

To calculate higher order corrections, we need to derive Feynman rules for the propagators and interactions. In contrast to the continuum formulation, the lattice regularisation causes some additional complications. First, the gauge invariant integration measure depends non-trivially on the gauge fields, resulting in additional vertices. Second, the regularisation generates infinite number of diagrams, which become more complex, as the number of legs increases.

Because of the finite lattice spacing, the momentum p is replaced by trigonometric functions, and hence lattice integrals are more difficult to calculate than the corresponding continuum ones. E.g., for a scalar field propagator we have

$$\frac{1}{\tilde{p}^2 + m^2}, \tag{A.7}$$

where

$$\tilde{p}^2 = \frac{4}{a}\sum_{i=1}^{3}\sin^2\left(\frac{ap_i}{2}\right) \tag{A.8}$$

Feynman rules for the vertices, derived up to the four gluon vertex, can be found, e.g., from [99, 100].

The calculation of next-to-leading order terms requires a two loop calculation. In three dimensions, it has been first computed in [101]. The diagrams needed are displayed in Fig. A.1. The integrands are rather complicated combinations of trigonometric functions. For example, the sunset diagram reads:

$$\begin{aligned} g_{\rm E}^2\frac{f_{abc}f_{abc}}{12}\int_{-\pi/a}^{\pi/a}\frac{{\rm d}^3p_1}{(2\pi)^3}\frac{{\rm d}^3q}{(2\pi)^3}\frac{{\rm d}^3r}{(2\pi)^3}\Big[\delta_{jk}\widetilde{(r-q)}_i\underset{\sim}{p}_j + \delta_{ik}\widetilde{(p-r)}_j\underset{\sim}{q}_k + \delta_{ij}\widetilde{(q-p)}_k\underset{\sim}{r}_i\Big] \\ \Big[-\delta_{jk}\widetilde{(q-r)}_i\underset{\sim}{p}_k - \delta_{ij}\widetilde{(p-q)}_j\underset{\sim}{r}_i - \delta_{ij}\widetilde{(p-q)}_k\underset{\sim}{q}_j\Big]\frac{\delta(p+q+r)}{\widetilde{p}^2\widetilde{q}^2\widetilde{r}^2}, \end{aligned} \tag{A.9}$$

where we used a notation

$$\widetilde{p}_i = \frac{2}{a}\sin\left(\frac{p_ia}{2}\right), \qquad \underset{\sim}{p}_i = \cos\left(\frac{p_ia}{2}\right). \tag{A.10}$$

One challenge is to reduce the integrals to a minimum set of master integrals, which then will be calculated numerically. In a two loop calculation of pure gauge theory this can be done

by hand, but for additional loop orders or more complicated theories automation is necessary. A pulchritudinous algorithm, which can be implemented, e.g., with FORM [102], has been presented in [62]. The sunset diagram reduces to

$$-g_{\mathrm{E}}^2 d_{\mathrm{A}} N_{\mathrm{c}} \left(-\frac{1}{96} + \frac{1}{8}\Sigma - \frac{3}{2}\Sigma^2 + 6\frac{\kappa_1}{(4\pi)^2} + \frac{2}{3}\frac{\kappa_5}{(4\pi)^2} \right), \tag{A.11}$$

where the constants are defined as

$$\Sigma = \frac{1}{\pi^2}\int_{-\frac{\pi}{2}}^{\frac{\pi}{2}} \mathrm{d}^3x \frac{1}{\sum_i \sin^2 x_i} = 3.175911535625\ldots \tag{A.12}$$

$$\kappa_1 = \frac{1}{4\pi^4}\int_{-\frac{\pi}{2}}^{\frac{\pi}{2}} \mathrm{d}^3x \mathrm{d}^3y \frac{\sin^2 x_i \sin^2(x_i+y_i)}{\sum_i \sin^2 x_i \sum_i \sin^2(x_i+y_i) \sum_i \sin^2 y_i} = 0.958382(1) \tag{A.13}$$

$$\kappa_5 = \frac{1}{\pi^4}\int_{-\frac{\pi}{2}}^{\frac{\pi}{2}} \mathrm{d}^3x \mathrm{d}^3y \frac{\sum_i \sin^2 x_i \sin^2(x_i+y_i) \sin^2 y_i}{\sum_i \sin^2 x_i \sum_i \sin^2(x_i+y_i) \sum_i \sin^2 y_i} = 1.013041(1). \tag{A.14}$$

An analytic expression has been found only for Σ [42]. The others have to be calculated numerically. Because the integrands are singular near the origin, the most straightforward method to calculate them is to use different lattice sizes and extrapolate to $N \to \infty$. There are some symmetries one can use to reduce the calculation time, but with a modern PC, a five decimal precision can be obtained without any tricks in less than 30min. Error estimation is challenging since all the errors are systematic. The most reliable method seems to be to test the sensitivity of the result with respect to the order of the fitting polynomial. If higher precision is required or the integrals are of higher dimensions, one can try to reduce the number of integration variables. Two of them can be removed with a standard trick, e.g, for Σ we can write,

$$\Sigma = \frac{1}{\pi^2}\int_{-\frac{\pi}{2}}^{\frac{\pi}{2}} \mathrm{d}^3x \frac{1}{\sum_i \sin^2 x_i} \tag{A.15}$$

$$= \pi \int_{-\frac{\pi}{2}}^{\frac{\pi}{2}} \mathrm{d}^3x \int_0^\infty \mathrm{d}\alpha \exp\left[-\alpha \sum_i \sin^2 x_i \right] \tag{A.16}$$

$$= \pi \int_0^\infty \mathrm{d}\alpha \left[e^{-\frac{1}{2}\alpha} I_0\left(\frac{\alpha}{2}\right) \right]^3, \tag{A.17}$$

where I_0 is the modified Bessel function. Another option is to use the coordinate space method described in [103].

Calculating all the diagrams of Fig. A.1, we obtain the 2-loop result

$$c_2 = -\frac{2}{3}\frac{d_A N_{\mathrm{c}}^2}{(4\pi)^2}\left(\frac{4\pi^2}{3N_{\mathrm{c}}^2} + \frac{\Sigma^2}{4} - \pi\Sigma - \frac{\pi^2}{2} + 4\kappa_1 + \frac{2}{3}\kappa_5 \right) \tag{A.18}$$

$$= d_A N_{\mathrm{c}}^2 \left(0.03327444(8) - \frac{1}{18}\frac{1}{N_{\mathrm{c}}^2} \right). \tag{A.19}$$

The tree loop term has been calculated in [97], where the authors have automatized the whole procedure from diagram generation to their numerical calculation. An additional complication is the need to derive the five and six gluon vertices. The result reads

$$c_3 = d_A N_{\mathrm{c}}^4 \left(0.0147397(3) - 0.04289464(7)\frac{1}{N_{\mathrm{c}}^2} + 0.04978944(1)\frac{1}{N_{\mathrm{c}}^4} \right). \tag{A.20}$$

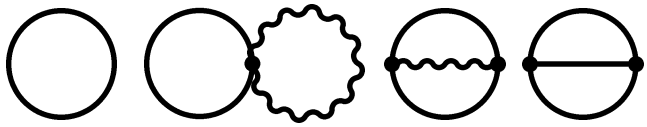

Figure A.2: The diagrams needed to calculate the continuum limit of condensates K_i

The four loop term has only been calculated at $N_c = 3$ using stochastic perturbation theory [70]. We note that the calculation requires an introduction of a mass to the gluon terms, which acts as an infrared cut off. The stochastic perturbation theory result reads

$$c_4'(N_c = 3) = 7.0 \pm 0.3. \tag{A.21}$$

A.2 Lattice integrals in EQCD

The massive propagator causes additional complications to the calculations since the integrals have to be expanded in m. However, the task is made easier by the fact that we only need contributions up to 2 loops. The needed Feynman rules are calculated in [93] and the needed diagrams are shown in Fig. A.2.

The derivative of the one loop graph with respect to m^2 is the tadpole graph

$$I(a,m) = \int_{-\pi/a}^{\pi/a} \frac{\mathrm{d}^3 p}{(2\pi)^3} \frac{1}{\tilde{p}^2 + m^2}. \tag{A.22}$$

A naive expansion in m^2 does not work, because the integrals in the higher terms would be infrared divergent. First, note that lattice degree of divergence $\mathrm{degr} I_F$, given by power count theorem of Reisz [104], is positive ($\mathrm{degr} I_F = 3 - 2 = 1$), which means that the naive continuum limit $\tilde{p}^2 \to p^2$ does not work. To obtain the leading order term, let us divide the integrand in to two parts.

$$I(a,m) = I(a,0) + \left[I(a,m) - I(a,0) \right]. \tag{A.23}$$

The first part, giving the leading order contribution, is easily computed and gives

$$I(a,0) = \frac{\Sigma}{4a\pi}. \tag{A.24}$$

The second part, which we denote by $I'(a,m)$, becomes

$$I'(a,m) = -m^2 \int_{-\pi/a}^{\pi/a} \frac{\mathrm{d}^3 p}{(2\pi)^3} \frac{1}{(\tilde{p}^2 + m^2)\tilde{p}^2}, \tag{A.25}$$

Now, $I'(a,m)$ has a negative $\mathrm{degr} I_F = 3 - 4 = -1$, and consequently the next order term is given by the corresponding continuum integral. Hence, we can proceed by dividing the integral again

$$I'(a,m) = I'(0,m) + \left[I'(a,m) - I'(0,m) \right], \tag{A.26}$$

where the first part is

$$I'(0,m) = -m^2 \int \frac{\mathrm{d}^3 p}{(2\pi)^3} \frac{1}{(p^2 + m^2)p^2} = -\frac{m}{4\pi}. \tag{A.27}$$

The higher order corrections (not needed here) can be calculated by continuing the procedure, which results in

$$I(a,m) = \frac{1}{4\pi}\left[\frac{\Sigma}{a} - m - \xi a m^2 + \mathcal{O}\left(a^2 m^3\right)\right], \tag{A.28}$$

where

$$\xi = \frac{1}{\pi^2}\left[\int_{-\frac{\pi}{2}}^{\frac{\pi}{2}} \mathrm{d}^3x \frac{1}{(\sum_i \sin^2 x_i)^2} - \int \mathrm{d}^3p \frac{1}{p^4}\right] = 0.15281(1) \tag{A.29}$$

The most complicated integral arising from the two-loop calculation is the sunset integral

$$H(a,m_1,m_2,m_3) = \int_{-\pi/a}^{\pi/a} \frac{\mathrm{d}^3p}{(2\pi)^3}\frac{\mathrm{d}^3q}{(2\pi)^3}\frac{1}{\tilde{p}^2+m_1^2}\frac{1}{\tilde{q}^2+m_2^2}\frac{1}{\widetilde{(p-q)}^2+m_3^2}, \tag{A.30}$$

Having a $\mathrm{degr} I_F = 6-6 = 0$, the leading order term H_0 contains the lattice contribution, but the logarithmic term has the same coefficient as the corresponding continuum integral (calculated, e.g., in [105]). Hence, we can write

$$H(a,m_1,m_2,m_3) = \frac{1}{16\pi^2}\left(\ln\frac{6}{a(m_1+m_2+m_3)} + \frac{1}{2} + \zeta + \mathcal{O}\left(am\right)\right), \tag{A.31}$$

where the remaining lattice coefficient needs an infrared regulator z

$$\zeta = \lim_{z\to 0}\left[\frac{1}{4\pi^4}\int_{-\pi/2}^{\pi/2}\frac{\mathrm{d}^3x\mathrm{d}^3y}{(\sum_i \sin^2 x_i + z^2)\sum_i \sin^2 y_i \sum_i \sin^2(x_i+y_i)} - \ln\frac{3}{z} - \frac{1}{2}\right], \tag{A.32}$$

and must be evaluated numerically. The result is $\zeta = 0.08848010(1)$.

After calculating all of the integrals with similar methods, subtracting the values of corresponding continuum integrals, and using equations (5.24) and (5.25), we obtain the needed numerical coefficients:

$$\begin{aligned}
\tilde{c}_1 &= \frac{d_\mathrm{A} N_\mathrm{c} \Sigma}{4\pi^2} \approx 0.1684873399,\\
\tilde{c}_2 &= \frac{N_\mathrm{c} d_\mathrm{A}}{(4\pi)^2} \approx 0.1519817755,\\
\tilde{c}_2' &= \zeta + \frac{\Sigma^4}{4} - \delta \approx 0.66796(1),\\
\bar{c}_2 &= \frac{5}{16\pi^2} \approx 0.0316628698900405,\\
\bar{c}_2' &= \zeta \approx 0.08848010(1),
\end{aligned} \tag{A.33}$$

where

$$\delta = \frac{1}{2\pi^4}\int_{-\pi/2}^{\pi/2}\mathrm{d}^3x\mathrm{d}^3y \frac{\sum_i \sin^2 x_i \sin^2(x_i+y_i)}{(\sum_i \sin^2 x_i)^2(\sum_i \sin^2(x_i+y_i))(\sum_i \sin^2 y_i)} \approx 1.942130(1). \tag{A.34}$$

Bibliography

[1] A. Hietanen, K. Kajantie, M. Laine, K. Rummukainen, and Y. Schröder, *Plaquette expectation value and gluon condensate in three dimensions*, JHEP **01** (2005) 013, hep-lat/0412008.

[2] A. Hietanen and A. Kurkela, *Plaquette expectation value and lattice free energy of three-dimensional SU(N(c)) gauge theory*, JHEP **11** (2006) 060, hep-lat/0609015.

[3] A. Hietanen and K. Rummukainen, *The diagonal and off-diagonal quark number susceptibility of high temperature and finite density QCD*, arXiv:0802.3979 [hep-lat].

[4] A. Hietanen, K. Kajantie, M. Laine, K. Rummukainen, and Y. Schröder, *Non-perturbative plaquette in 3d pure SU(3)*, PoS **LAT2005** (2006) 174, hep-lat/0509107.

[5] A. Hietanen and K. Rummukainen, *Quark number susceptibility at high temperature*, PoS **LAT2006** (2006) 137, hep-lat/0610111.

[6] A. Hietanen and K. Rummukainen, *Quark number susceptibility of high temperature and finite density QCD*, PoS **LAT2007** (2007) 192, arXiv:0710.5058 [hep-lat].

[7] M. Gell-Mann, *A Schematic Model of Baryons and Mesons*, Phys. Lett. **8** (1964) 214–215.

[8] G. Zweig, *An SU(3) model for strong interaction symmetry and its breaking. 2*, . CERN-TH-412.

[9] M. Y. Han and Y. Nambu, *Three-triplet model with double SU(3) symmetry*, Phys. Rev. **139** (1965) B1006–B1010.

[10] O. W. Greenberg, *Spin and Unitary Spin Independence in a Paraquark Model of Baryons and Mesons*, Phys. Rev. Lett. **13** (1964) 598–602.

[11] D. J. Gross and F. Wilczek, *Ultraviolet behavior of non-abelian gauge theories*, Phys. Rev. Lett. **30** (1973) 1343–1346.

[12] H. D. Politzer, *Reliable perturbative results for strong interactions?*, Phys. Rev. Lett. **30** (1973) 1346–1349.

[13] K. G. Wilson, *Confinement of quarks*, Phys. Rev. **D10** (1974) 2445–2459.

[14] F. Karsch, *Recent lattice results on finite temperature and density QCD, part I*, arXiv:0711.0656 [hep-lat].

[15] F. Karsch, *Recent lattice results on finite temerature and density QCD, part II*, arXiv:0711.0661 [hep-lat].

[16] Z. Fodor, *QCD Thermodynamics*, arXiv:0711.0336 [hep-lat].

[17] M. Gyulassy and L. McLerran, *New forms of QCD matter discovered at RHIC*, Nucl. Phys. **A750** (2005) 30–63, nucl-th/0405013.

[18] M. Cheng *et al.*, *The qcd equation of state with almost physical quark masses*, arXiv:0710.0354 [hep-lat].

[19] A. D. Linde, *Infrared problem in thermodynamics of the yang-mills gas*, Phys. Lett. **B96** (1980) 289.

[20] M. Asakawa, U. W. Heinz, and B. Muller, *Fluctuation probes of quark deconfinement*, Phys. Rev. Lett. **85** (2000) 2072–2075, hep-ph/0003169.

[21] S. Jeon and V. Koch, *Charged particle ratio fluctuation as a signal for qgp*, Phys. Rev. Lett. **85** (2000) 2076–2079, hep-ph/0003168.

[22] J. I. Kapusta, *Finite temperature field theory*, .

[23] M. E. Peskin and D. V. Schroeder, *An Introduction to quantum field theory*, . Reading, USA: Addison-Wesley (1995) 842 p.

[24] L. D. Faddeev and V. N. Popov, *Feynman diagrams for the yang-mills field*, Phys. Lett. **B25** (1967) 29–30.

[25] E. Braaten and A. Nieto, *Free Energy of QCD at High Temperature*, Phys. Rev. **D53** (1996) 3421–3437, hep-ph/9510408.

[26] E. V. Shuryak, *Quark-gluon plasma and hadronic production of leptons, photons and psions*, Phys. Lett. **B78** (1978) 150.

[27] S. A. Chin, *Transition to hot quark matter in relativistic heavy ion collision*, Phys. Lett. **B78** (1978) 552–555.

[28] J. I. Kapusta, *Quantum chromodynamics at high temperature*, Nucl. Phys. **B148** (1979) 461–498.

[29] T. Toimela, *The next term in the thermodynamic potential of qcd*, Phys. Lett. **B124** (1983) 407.

[30] P. Arnold and C.-x. Zhai, *The three loop free energy for high temperature qed and qcd with fermions*, Phys. Rev. **D51** (1995) 1906–1918, hep-ph/9410360.

[31] C.-x. Zhai and B. M. Kastening, *The free energy of hot gauge theories with fermions through g**5*, Phys. Rev. **D52** (1995) 7232–7246, hep-ph/9507380.

[32] K. Kajantie, M. Laine, K. Rummukainen, and Y. Schröder, *The pressure of hot qcd up to g**6 ln(1/g)*, Phys. Rev. **D67** (2003) 105008, hep-ph/0211321.

[33] A. Vuorinen, *The pressure of qcd at finite temperatures and chemical potentials*, Phys. Rev. **D68** (2003) 054017, hep-ph/0305183.

[34] F. J. Dyson, *Divergence of perturbation theory in quantum electrodynamics*, Phys. Rev. **85** (1952) 631–632.

[35] B. C. Odom, D. Hanneke, B. D'Urso, and G. Gabrielse, *New Measurement of the Electron Magnetic Moment Using a One-Electron Quantum Cyclotron*, Phys. Rev. Lett. **97** (2006) 030801.

[36] K. Kajantie, M. Laine, K. Rummukainen, and Y. Schröder, *Four-loop vacuum energy density of the SU(N(c)) + adjoint Higgs theory*, JHEP **04** (2003) 036, hep-ph/0304048.

[37] P. H. Ginsparg, *First order and second order phase transitions in gauge theories at finite temperature*, Nucl. Phys. **B170** (1980) 388.

[38] T. Appelquist and R. D. Pisarski, *High-temperature yang-mills theories and three-dimensional quantum chromodynamics*, Phys. Rev. **D23** (1981) 2305.

[39] D. J. Gross, R. D. Pisarski, and L. G. Yaffe, *QCD and Instantons at Finite Temperature*, Rev. Mod. Phys. **53** (1981) 43.

[40] N. P. Landsman, *Limitations to dimensional reduction at high temperature*, Nucl. Phys. **B322** (1989) 498.

[41] K. Farakos, K. Kajantie, K. Rummukainen, and M. E. Shaposhnikov, *3-D physics and the electroweak phase transition: Perturbation theory*, Nucl. Phys. **B425** (1994) 67–109, hep-ph/9404201.

[42] K. Farakos, K. Kajantie, K. Rummukainen, and M. E. Shaposhnikov, *3-d physics and the electroweak phase transition: A Framework for lattice Monte Carlo analysis*, Nucl. Phys. **B442** (1995) 317–363, hep-lat/9412091.

[43] E. Braaten and A. Nieto, *Effective field theory approach to high temperature thermodynamics*, Phys. Rev. **D51** (1995) 6990–7006, hep-ph/9501375.

[44] A. Gynther and M. Vepsälainen, *Pressure of the standard model near the electroweak phase transition*, JHEP **03** (2006) 011, hep-ph/0512177.

[45] A. Gynther and M. Vepsälainen, *Pressure of the standard model at high temperatures*, JHEP **01** (2006) 060, hep-ph/0510375.

[46] M. Vepsälainen, *Mesonic screening masses at high temperature and finite density*, JHEP **03** (2007) 022, hep-ph/0701250.

[47] A. Gynther, *The electroweak phase diagram at finite lepton number density*, Phys. Rev. **D68** (2003) 016001, hep-ph/0303019.

[48] M. Laine and Y. Schröder, *Two-loop QCD gauge coupling at high temperatures*, JHEP **03** (2005) 067, hep-ph/0503061.

[49] K. Kajantie, M. Laine, K. Rummukainen, and Y. Schröder, *How to resum long-distance contributions to the QCD pressure?*, Phys. Rev. Lett. **86** (2001) 10–13, hep-ph/0007109.

[50] A. Hart, M. Laine, and O. Philipsen, *Static correlation lengths in qcd at high temperatures and finite densities*, Nucl. Phys. **B586** (2000) 443–474, hep-ph/0004060.

[51] A. Hart, M. Laine, and O. Philipsen, *Testing imaginary vs. real chemical potential in finite- temperature QCD*, Phys. Lett. **B505** (2001) 141–148, hep-lat/0010008.

[52] T. Appelquist and J. Carazzone, *Infrared Singularities and Massive Fields*, Phys. Rev. **D11** (1975) 2856.

[53] S. Chapman, *A New dimensionally reduced effective action for QCD at high temperature*, Phys. Rev. **D50** (1994) 5308–5313, hep-ph/9407313.

[54] A. Vuorinen, *Quark number susceptibilities of hot qcd up to g**6 ln(g)*, Phys. Rev. **D67** (2003) 074032, hep-ph/0212283.

[55] A. Vuorinen, *The pressure of QCD at finite temperature and quark number density*, hep-ph/0402242.

[56] A. Gynther, M. Laine, Y. Schröder, C. Torrero, and A. Vuorinen, *Four-loop pressure of massless O(N) scalar field theory*, JHEP **04** (2007) 094, hep-ph/0703307.

[57] S. Datta and S. Gupta, *Dimensional reduction and screening masses in pure gauge theories at finite temperature*, Nucl. Phys. **B534** (1998) 392–416, hep-lat/9806034.

[58] A. Ipp, K. Kajantie, A. Rebhan, and A. Vuorinen, *The pressure of deconfined QCD for all temperatures and quark chemical potentials*, Phys. Rev. **D74** (2006) 045016, hep-ph/0604060.

[59] A. Vuorinen and L. G. Yaffe, *Z(3)-symmetric effective theory for SU(3) Yang-Mills theory at high temperature*, Phys. Rev. **D74** (2006) 025011, hep-ph/0604100.

[60] K. Kajantie, M. Laine, A. Rajantie, K. Rummukainen, and M. Tsypin, *The phase diagram of three-dimensional SU(3) + adjoint Higgs theory*, JHEP **11** (1998) 011, hep-lat/9811004.

[61] K. Kajantie, M. Laine, K. Rummukainen, and M. E. Shaposhnikov, *3d SU(N) + adjoint Higgs theory and finite-temperature QCD*, Nucl. Phys. **B503** (1997) 357–384, hep-ph/9704416.

[62] A. Kurkela, *Framework for non-perturbative analysis of a Z(3)- symmetric effective theory of finite temperature QCD*, Phys. Rev. **D76** (2007) 094507, arXiv:0704.1416 [hep-lat].

[63] A. Kurkela, *Z(3)-symmetric effective theory of hot QCD*, PoS **LAT2007** (2007) 199, arXiv:0711.1796 [hep-lat].

[64] P. de Forcrand, A. Kurkela, and A. Vuorinen, *Center-Symmetric Effective Theory for High-Temperature SU(2) Yang-Mills Theory*, arXiv:0801.1566 [hep-ph].

[65] G. 't Hooft, *A planar diagram theory for strong interactions*, Nucl. Phys. **B72** (1974) 461.

[66] B. Bringoltz and M. Teper, *The pressure of the SU(N) lattice gauge theory at large- N*, Phys. Lett. **B628** (2005) 113–124, hep-lat/0506034.

[67] H. B. Meyer, *The spectrum of SU(N) gauge theories in finite volume*, JHEP **03** (2005) 064, hep-lat/0412021.

[68] R. Narayanan and H. Neuberger, *A survey of large N continuum phase transitions*, arXiv:0710.0098 [hep-lat].

[69] G. D. Moore, *O(a) errors in 3-D SU(N) Higgs theories*, Nucl. Phys. **B523** (1998) 569–593, hep-lat/9709053.

[70] F. Di Renzo, M. Laine, V. Miccio, Y. Schröder, and C. Torrero, *The leading non-perturbative coefficient in the weak- coupling expansion of hot QCD pressure*, JHEP **07** (2006) 026, hep-ph/0605042.

[71] C. P. Korthals Altes and H. B. Meyer, *Hot QCD, k-strings and the adjoint monopole gas model*, hep-ph/0509018.

[72] N. Metropolis, A. W. Rosenbluth, M. N. Rosenbluth, A. H. Teller, and E. Teller, *Equation of state calculations by fast computing machines*, J. Chem. Phys. **21** (1953) 1087–1092.

[73] M. Creutz, *Monte Carlo Study of Quantized SU(2) Gauge Theory*, Phys. Rev. **D21** (1980) 2308–2315.

[74] A. D. Kennedy and B. J. Pendleton, *Improved Heat Bath Method for Monte Carlo Calculations in Lattice Gauge Theories*, Phys. Lett. **B156** (1985) 393–399.

[75] E. Pietarinen, *String Tension in SU(3) Lattice Gauge Theory*, Nucl. Phys. **B190** (1981) 349.

[76] F. R. Brown and T. J. Woch, *Overrelaxed Heat Bath and Metropolis Algorithms for Accelerating Pure Gauge Monte Carlo Calculations*, Phys. Rev. Lett. **58** (1987) 2394.

[77] P. de Forcrand and O. Jahn, *Monte Carlo overrelaxation for SU(N) gauge theories*, hep-lat/0503041.

[78] J. Kiskis, R. Narayanan, and H. Neuberger, *Does the crossover from perturbative to nonperturbative physics in QCD become a phase transition at infinite N?*, Phys. Lett. **B574** (2003) 65–74, hep-lat/0308033.

[79] M. Luscher, *Volume Dependence of the Energy Spectrum in Massive Quantum Field Theories. 1. Stable Particle States*, Commun. Math. Phys. **104** (1986) 177.

[80] M. J. Teper, *SU(N) gauge theories in 2+1 dimensions*, Phys. Rev. **D59** (1999) 014512, hep-lat/9804008.

[81] B. Lucini and M. Teper, *SU(N) gauge theories in 2+1 dimensions: Further results*, Phys. Rev. **D66** (2002) 097502, hep-lat/0206027.

[82] M. Laine and O. Philipsen, *The non-perturbative QCD Debye mass from a Wilson line operator*, Phys. Lett. **B459** (1999) 259–264, hep-lat/9905004.

[83] R. V. Gavai, S. Gupta, and P. Majumdar, *Susceptibilities and screening masses in two flavor QCD*, Phys. Rev. **D65** (2002) 054506, hep-lat/0110032.

[84] R. V. Gavai and S. Gupta, *The continuum limit of quark number susceptibilities*, Phys. Rev. **D65** (2002) 094515, hep-lat/0202006.

[85] C. R. Allton *et al.*, *The equation of state for two flavor QCD at non-zero chemical potential*, Phys. Rev. **D68** (2003) 014507, hep-lat/0305007.

[86] C. R. Allton *et al.*, *Thermodynamics of two flavor QCD to sixth order in quark chemical potential*, Phys. Rev. **D71** (2005) 054508, hep-lat/0501030.

[87] C. Bernard *et al.*, *QCD thermodynamics with 2+1 flavors at nonzero chemical potential*, Phys. Rev. **D77** (2008) 014503, arXiv:0710.1330 [hep-lat].

[88] **MILC** Collaboration, C. Bernard *et al.*, *QCD thermodynamics with three flavors of improved staggered quarks*, Phys. Rev. **D71** (2005) 034504, hep-lat/0405029.

[89] J. P. Blaizot, E. Iancu, and A. Rebhan, *Quark number susceptibilities from HTL-resummed thermodynamics*, Phys. Lett. **B523** (2001) 143–150, hep-ph/0110369.

[90] O. Philipsen, *Lattice QCD at finite temperature and density*, Eur. Phys. J. Spec. Top. **152** (2007) 29–60, arXiv:0708.1293 [hep-lat].

[91] **ALPHA** Collaboration, M. Della Morte *et al.*, *Computation of the strong coupling in QCD with two dynamical flavours*, Nucl. Phys. **B713** (2005) 378–406, hep-lat/0411025.

[92] **DIK** Collaboration, V. G. Bornyakov *et al.*, *Finite temperature Lattice QCD with two flavors of improved Wilson fermions*, PoS **LAT2007** (2007) 171, arXiv:0711.1427 [hep-lat].

[93] M. Laine and A. Rajantie, *Lattice-continuum relations for 3d SU(N)+Higgs theories*, Nucl. Phys. **B513** (1998) 471–489, hep-lat/9705003.

[94] F. Karsch, S. Ejiri, and K. Redlich, *Hadronic fluctuations in the QGP*, Nucl. Phys. **A774** (2006) 619–622, hep-ph/0510126.

[95] M. Laine and M. Vepsälainen, *Mesonic correlation lengths in high-temperature QCD*, JHEP **02** (2004) 004, hep-ph/0311268.

[96] M. Laine, *Exact relation of lattice and continuum parameters in three-dimensional SU(2) + Higgs theories*, Nucl. Phys. **B451** (1995) 484–504, hep-lat/9504001.

[97] H. Panagopoulos, A. Skouroupathis, and A. Tsapalis, *Free energy and plaquette expectation value for gluons on the lattice, in three dimensions*, Phys. Rev. **D73** (2006) 054511, hep-lat/0601009.

[98] M. Creutz, *Quarks, gluons and lattices*, . Cambridge, Uk: Univ. Pr. (1983) 169 P. (Cambridge Monographs On Mathematical Physics).

[99] H. J. Rothe, *Lattice gauge theories: An Introduction*, World Sci. Lect. Notes Phys. **59** (1997) 1–512.

[100] S. Capitani, *Lattice perturbation theory*, Phys. Rept. **382** (2003) 113–302, hep-lat/0211036.

[101] U. M. Heller and F. Karsch, *One Loop Perturbative Calculation of Wilson Loops on Finite Lattices*, Nucl. Phys. **B251** (1985) 254.

[102] J. A. M. Vermaseren, *New features of FORM*, math-ph/0010025.

[103] M. Luscher and P. Weisz, *Coordinate space methods for the evaluation of Feynman diagrams in lattice field theories*, Nucl. Phys. **B445** (1995) 429–450, `hep-lat/9502017`.

[104] T. Reisz, *A power counting theorem for Feynman integrals on the lattice*, Commun. Math. Phys. **116** (1988) 81.

[105] A. K. Rajantie, *Feynman diagrams to three loops in three-dimensional field theory*, Nucl. Phys. **B480** (1996) 729–752, `hep-ph/9606216`.